ISSN 0006-2979, Biochemistry (Moscow), 2019, Vol. 84, Suppl. 1, pp. S69-S88. © Pleiades Publishing, Ltd., 2019.
Russian Text © E. A. Shirshin, B. P. Yakimov, M. E. Darvin, N. P. Omelyanenko, S. A. Rodionov, Y. I. Gurfinkel, J. Lademann, V. V. Fadeev, A. V. Priezzhev, 2019, published in Uspekhi Biologicheskoi Khimii, 2019, Vol. 59, pp. 139-180.

REVIEW

Label-Free Multiphoton Microscopy: The Origin of Fluorophores and Capabilities for Analyzing Biochemical Processes

E. A. Shirshin[1,2,a]*, B. P. Yakimov[1], M. E. Darvin[3], N. P. Omelyanenko[4], S. A. Rodionov[4], Y. I. Gurfinkel[5], J. Lademann[3], V. V. Fadeev[1], and A. V. Priezzhev[1]

[1]Lomonosov Moscow State University, Faculty of Physics, 119991 Moscow, Russia
[2]Institute of Spectroscopy, Russian Academy of Sciences, 108840 Troitsk, Moscow, Russia
[3]Center of Experimental and Applied Cutaneous Physiology, Department of Dermatology, Venerology and Allergology, Charité – Universitätsmedizin Berlin, corporate member of Freie Universität Berlin, Humboldt-Universität zu Berlin, and Berlin Institute of Health, Charitéplatz 1, 10117 Berlin, Germany
[4]N. N. Priorov National Medical Research Center of Traumatology and Orthopaedics, 127299 Moscow, Russia
[5]Medical Scientific-Educational Center of Lomonosov Moscow State University, 119192 Moscow, Russia
[a]e-mail: shirshin@lid.phys.msu.ru

Received August 22, 2018
Revised September 25, 2018
Accepted September 25, 2018

Abstract—Multiphoton microscopy (MPM) is a method of molecular imaging and specifically of intravital imaging that is characterized by high spatial resolution in combination with a greater depth of penetration into the tissue. MPM is a multimodal method based on detection of nonlinear optical signals – multiphoton fluorescence and optical harmonics – and also allows imaging with the use of the parameters of fluorescence decay kinetics. This review describes and discusses photophysical processes within major reporter molecules used in MPM with endogenous contrasts and summarizes several modern experiments that illustrate the capabilities of label-free MPM for molecular imaging of biochemical processes in connective tissue and cells.

DOI: 10.1134/S0006297919140050

Keywords: molecular imaging, multiphoton microscopy, FLIM, autofluorescence, optical harmonic generation, fluorophores

Optical diagnostic methods are now being actively developed that make it possible to study processes in living organisms at the molecular and cellular levels. One of these methods is multiphoton microscopy (MPM), or multiphoton tomography [1] with visualization of fluorescence decay time (fluorescence lifetime imaging, FLIM [2, 3]). The major advantage of MPM as a molecular imaging method is its high spatial resolution combined with a greater depth of tissue penetration [4, 5]. MPM is used in immunology, oncology research, and neurobiology while applying various probes to increase signal intensity, its specificity, and imaging depth [4, 6-8]. However, exogenous probes are technically difficult to apply for studying human tissues *in vivo*, and in this case using endogenous sources of informative signals greatly simplifies the problem. Moreover, it turned out that in a number of cases using an endogenous signal allows not only to visualize the distribution of molecules of a particular type in tissue, but also to investigate the biochemical processes occurring within it. In particular, so-called fluorescent metabolic imaging has become widespread [9, 10].

In MPM, the sources of endogenous signals include fluorophore molecules emitting fluorescence under multiphoton excitation ("multiphoton fluorescence"), anisotropic macromolecules and structures generating

Abbreviations: AF, autofluorescence; AGEs, advanced glycation endproducts; CARS, coherent anti-Stokes Raman scattering; FAD, flavin adenine dinucleotide; FLIM, fluorescence lifetime imaging; FP, flavoprotein; IR, infrared; MI, metabolic imaging; MPM, multiphoton microscopy; NAD, nicotinamide adenine dinucleotide; NAD^F/NAD^B, free/bound form of NAD; NADP, nicotinamide adenine dinucleotide phosphate; OP, oxidative phosphorylation; ROS, reactive oxygen species; SC, stem cells; SHG, second harmonic generation; TCSPC, time-correlated single photon counting; THG, third harmonic generation; TP, two-photon; UV, ultraviolet.

* To whom correspondence should be addressed.

optical harmonics; any molecules in which intramolecular oscillations can be measured by the method of coherent anti-Stokes Raman spectroscopy [11]. Endogenous fluorescence (or autofluorescence (AF)) is a classical effect that has been used in biomedical diagnostics for decades. and it is described in detail in monographs and reviews [12-14]. In general, MPM uses the same groups of fluorophores as classical fluorescence spectroscopy does, but there is a number of features underlying the approaches to studying biochemical processes and molecular imaging. The generation of optical harmonics is a nonlinear effect that allows visualization of structures having a specific organization – for example, type I collagen and cells in tissue [15]. The use of multimodal detection in MPM, based on simultaneous measuring of AF, harmonic generation, and FLIM, may significantly extend the scope of molecular imaging both for fundamental research of biochemical processes and for *in vivo* diagnostics.

The aim of this review is to describe the photophysical processes within the major reporter molecules used in MPM with endogenous contrasts (label-free), as well as to present several modern experiments illustrating the possibilities of label-free MPM for molecular imaging of biochemical processes in connective tissue.

THE MULTIPHOTON MICROSCOPY METHOD

Nonlinear microscopy. Optical microscopy uses light as probing radiation – conclusions regarding the structure of the analyzed object are drawn according to the characteristics of its interaction with matter. Interaction of light with matter can be represented as follows. Light falling on the material medium results in a redistribution of electron density of atoms. Light is absorbed, and electron density fluctuations themselves become sources of secondary light waves. The characteristic size of atoms and their dense packing (~10^{-8} cm) are significantly less than optical range wavelength (~10^{-4} cm), allowing to introduce such characteristic as polarization $\vec{P}$ – dipole moment per unit volume of the medium [16]. Nonlinear optical processes can be also described using the polarization vector [17].

In the simplest case, polarization $\vec{P}$ linearly depends on the intensity of the incident light field. Therefore, the intensity of the detected signal depends linearly on the intensity of pumping, and if the incident light field has a frequency ω, then the polarization of the matter also oscillates at the frequency ω, and the secondary radiation generated by it has the same wavelength. Such an approximation is valid at very low intensities of the incident field intensity compared to the intra-atomic field ($I << I_{atomic}$ ~ $5 \cdot 10^{16}$ W/cm^2).

Methods of optical microscopy that use linear (single-photon) processes to create contrast are not applicable to imaging of deep layers of tissue: sharp images can only be obtained near the surface, since the effect of multiple light scattering prevails in deeper layers, making images blurry [4, 18]. Methods of nonlinear optical microscopy have a number of advantages that make them suitable for high-resolution imaging in tissues at depths exceeding 500 μm at certain conditions [19].

Under illumination of a medium by high-intensity (laser) radiation, nonlinearity of the dependence of polarization on the intensity of the electric field of the light wave begins to manifest:

$$\vec{P}(\vec{E}) = \hat{\chi}^{(1)}\vec{E} + \hat{\chi}^{(2)}\vec{E}^2 + \hat{\chi}^{(3)}\vec{E}^3 + \cdots, \quad (1)$$

where $\hat{\chi}^{(1)}$ is linear susceptibility; $\hat{\chi}^{(2)}$, $\hat{\chi}^{(3)}$ – nonlinear susceptibilities of the second, third, etc. orders. Accordingly, the intensity of the secondary radiation can nonlinearly (quadratically, cubically, etc.) depend on the intensity of the incident radiation.

The major nonlinear optical effects observed and used in microscopy are: the processes of the second (SHG, $\hat{\chi}^{(2)}$) and third (THG, $\hat{\chi}^{(3)}$) harmonics generation, the process of two-photon (TP) fluorescence excitation ($\hat{\chi}^{(3)}$), the process of coherent anti-Stokes Raman scattering (CARS, $\hat{\chi}^{(3)}$) [4].

Two-photon fluorescence excitation. TP fluorescence excitation is a nonlinear third-order effect consisting of "simultaneous" (time of interaction is ~0.5 fs) absorption of two photons by molecule and the subsequent emission of fluorescence [4, 5, 20]. Fluorescence itself is always a single-photon process, and the spectral and temporal characteristics of a fluorescence signal after multiphoton absorption do not differ from that of single-photon-induced fluorescence. Quantum-mechanical description of the TP absorption process is given in the literature [17, 21].

The process of TP absorption can be represented as follows: the "first" incoming photon of incident radiation can excite molecule from the ground state *g* to an intermediate virtual state *v*, and after that, the "second" photon has the probability to excite the molecule from the virtual excited state to a real excited state *e* (Fig. 1a). Therefore, fluorescence intensity, I_{TPEF}, will be proportional to the square of pump intensity, I_P, and to the cross section of TP absorption, $\sigma^{(2)}$:

$$I_{TPEF} \sim \sigma^{(2)} I_p^2. \quad (2)$$

The cross section of TP absorption, which has a dimension of cm^4·s, can be estimated as:

$$\sigma^{(2)} \sim \sigma_{gv}^{(1)} \sigma_{ve}^{(1)} \tau_v, \quad (3)$$

where $\sigma_{gv}^{(1)}$, $\sigma_{ve}^{(1)}$ – cross sections of single-photon absorptions, the characteristic value of which is 10^{-17}-10^{-16} cm^2, and τ_v is the lifetime of the virtual state which, which for

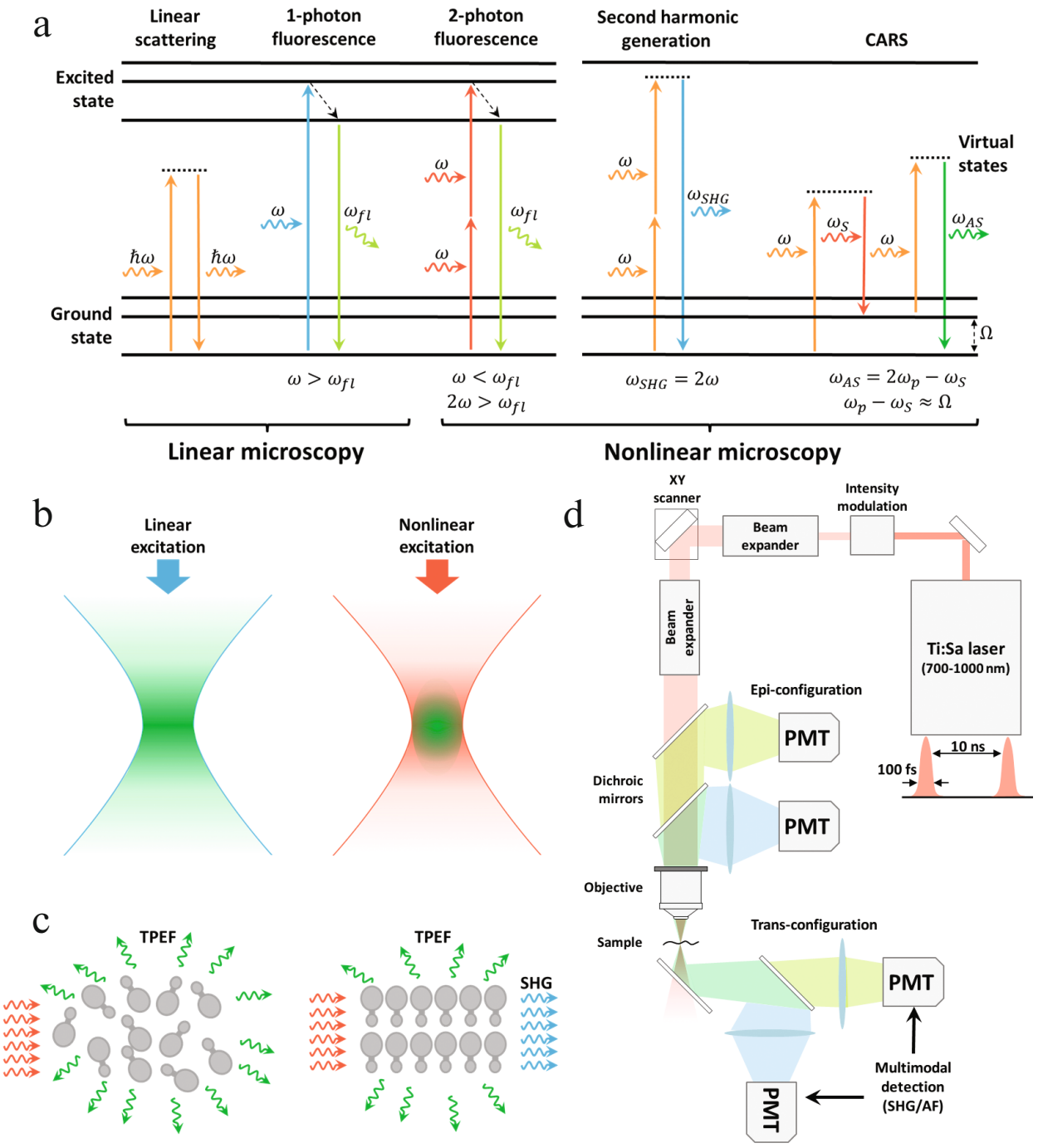

Fig. 1. a) Diagrams of linear and nonlinear optical processes. Note that in the case of linear scattering, generation of the second harmonic, and CARS, no electronic excitation of sample molecules occurs. b) Spatial localization of the signal with linear and nonlinear excitation. With linear excitation, the signal is generated from the entire volume, while with nonlinear excitation, the signal is generated only from a small (of the order of a femtoliter) region. c) Generation of TP-excited fluorescence (TPEF) and second harmonic (SHG). Fluorescence emission is isotropic and does not depend on the macroscopic ordering of a sample (left). For effective radiation at the frequency of the second harmonic, macroscopic ordering is required (right). d) Schematic diagram of a multiphoton microscope. PMT, photomultiplier tubes. Adapted from [4] by permission from Springer Nature Customer Service Centre GmbH: Springer Nature, Nature Methods.

photons with the frequency ω and transition frequency ω_{ev} can be estimated from Heisenberg's uncertainty ratio as $\tau_v \sim 1/|\omega_{ev} - \omega| \approx 10^{-16}$-$10^{-15}$ s. Therefore, the cross section of TP absorption is of the order of $\sigma^{(2)} \approx 10^{-49}$ cm^4·s. A generalization for *n*-photon absorption can be carried out in a similar way.

For TP excitation, it is usually sufficient to double the wavelength of the radiation used for single-photon

excitation. However, in addition to the estimate of TP absorption cross section given above (Eq. (3)), it is important to remember that selection rules for TP processes differ from those for single-photon processes. For example, single-photon transitions between states of different parity are allowed in symmetric molecules, while TP transitions are possible only between states of the same parity – as a result, the shapes of single-photon and TP absorption spectra sometimes may differ significantly [22].

Generation of optical harmonics. The effect of generation of optical harmonics is fundamentally different from multiphoton absorption. Experimentally, generation of the second and third optical harmonics is the easiest to observe. In these processes, two (three) photons are "simultaneously" scattered by the electrons of the molecule, turning into one photon with the energy that is exactly two (three) times higher (Fig. 1a). Generation of harmonics, being an effect of nonlinear scattering, does not require absorption of the incident wave in a sample; however, it is enhanced due to a resonant increase in polarizability if the radiation frequency approaches the frequency of electronic transition of molecules [4, 23].

It can be demonstrated that intense scattering with the doubled frequency will be observed if a molecule does not exhibit inversion symmetry. However, the absence of inversion symmetry for molecules is not sufficient for generation of the second harmonic; it is also essential that such asymmetry is preserved in macrovolume. We should note that such a restriction on the absence of inversion symmetry is required only for effective generation of even optical harmonics [17, 21].

If scattering on a doubled frequency occurs for volumetrically disordered molecules, then a fraction of the waves will interfere destructively (and the signal will be low in intensity), and in the case of an ordered molecule arrangement, the scattered radiation will be emitted coherently – such coherent propagation is called SHG [21, 24]. Coherence also implies that optical harmonics will be generated effectively only in certain directions, in contrast to AF (Fig. 1c).

Coherent anti-Stokes Raman scattering. Another nonlinear optical process that is still quite rarely used in practice but is promising for molecular imaging is coherent anti-Stokes Raman scattering (CARS). A diagram of this process is shown in Fig. 1a. The object is irradiated by incident radiation containing three waves, two of which usually possess the same frequency ω_p, and the third one, denoted as the Stokes wave, has the frequency ω_S. Interacting on cubic polarizability, these waves "generate" several frequency polarization components, which become sources of secondary waves with the frequencies of these components. CARS uses a component with the frequency $\omega A_S = 2\omega_p - \omega_S$ [25-27], the frequency of which is higher than that of incident waves, allowing to call it anti-Stokes. CARS spectroscopy is based on the effect of resonant increase in cubic polarizability and, as a result, in radiation intensity on a combination (anti-Stokes) frequency with tuning of the difference between the frequencies of the incident waves to the frequency of intramolecular oscillations: $\omega_p - \omega_S \approx \Omega$. Therefore, CARS spectroscopy can selectively visualize molecules with specific chemical bonds. During instrumental implementation of CARS, a laser is used with a tuning of one of the frequencies of incident radiation. The main advantage of CARS in comparison with spontaneous Raman scattering (SRS) is its greater sensitivity (by 5-8 orders of magnitude).

Advantages of nonlinear microscopy for molecular imaging and characteristic parameters of the applied setups. As noted earlier, methods of nonlinear optical microscopy have several advantages compared to linear microscopy.

First, for excitation of molecules that absorb in the UV and short-wavelength part of the visible range (λ ~ 350-500 nm), radiation in the red region of visible light and the near-IR range can be used (λ_{ex} ~ 700-1000 nm). The radiation of such wavelengths has a greater penetration depth compared to visible light due to lower scattering – the characteristic value of the optical path of the visible light in skin will be in the order of 100 μm, while at the wavelength of 1000 nm (near-IR range), this length will be in the order of 600 μm [28]. Second, multiphoton absorption spectra are less structured and wider than single-photon absorption spectra – often, no selection of optimal conditions for fluorescence excitation is required [29]. Third, since nonlinear processes have power dependence on the intensity of the incident radiation, the signal is generated only in the focal plane of the lens from a volume of the order of a femtoliter (Fig. 1b). Due to this, potential photodamage is limited only to the focal volume and does not take place above and below the lens focus [30]. Additionally, by generating a signal only from the focal plane and with a larger penetration depth, it is possible to scan samples three-dimensionally [4, 31].

Note that despite the lower value of the scattering coefficient in the near-IR range, the number of ballistic (non-scattered) pump photons in tissues decays exponentially with penetration depth – the capabilities of MPM in penetrating tissue are limited. For example, the signal of generated two-photon fluorescence F is determined as

$$F \propto \left[P_0 \exp\left(-z/l_s^{(ex.)}\right)\right]^2,$$

where P_0 – power of excitation radiation on the sample surface, $l_s^{(ex.)}$ – free path length of a photon scattered on the excitation wavelength. Consequently, the maximum penetration depth can be estimated as:

$$z_{max} \approx l_s^{(ex.)} \ln\left(\alpha P_0 \frac{T}{\tau}\sqrt{\Phi(z_{max})}\right), \qquad (4)$$

where Φ is the fraction of fluorescence photons that were detected, α – the parameter characterizing the efficiency of fluorophores' radiation and noise characteristics of the detector, τ and $1/T$ – characteristic pulse length and repetition rate of the pulses [19]. Therefore, improving the efficiency of light detection or increasing the power of excitation radiation will only result in an insignificant increase in the maximum penetration depth (Eq. (4)), and at the same time, an increase in power densities may result in photochemical damage of metabolites and thermal tissue damage. Given this, the maximum depth of MPM using the signal of endogenous fluorophores can be estimated as ~200 μm [18]. A significant increase in the penetration depth (up to 1.6 mm) may be achieved by shifting the excitation radiation to the long-wavelength region (1000-1300 nm) [32, 33]; however, an increase in the excitation radiation wavelength can result in a decrease of the detected signal due to the low cross section of nonlinear optical processes in the long wavelength region. It should also be noted that the MPM penetration depth is limited by the presence of a weak background fluorescence signal generated outside of the focal plane. A detailed study of the limitations of MPM in tissue penetration was carried out, for example, in [34].

Here is a brief description of the main parameters of experimental setups used for nonlinear optical microscopy. A detailed description can be found, for example, in the studies [31, 35]. The principle of operation of a multiphoton microscope is in many respects similar to that of a confocal laser scanning microscope. The main difference is related to radiation sources. A tunable wavelength (700-1000 nm) titanium-sapphire laser is commonly used as a radiation source. The characteristic duration of radiation pulses is ~100 fs, which makes it possible to achieve peak intensities of the order of 10^{13} W/cm^2 in the focal plane by spatial focusing with lenses of a large numerical aperture. Such intensities are sufficient to generate nonlinear optical signals.

A typical optical path of a multiphoton microscope is as follows. The laser beam passes through an intensity modulator, after which the beam is expanded with a telescopic system and hits the galvanic scanner controlling the beam position in the XY plane (Fig. 1d). The scanning rate can reach ~30 frames per second [36]. After the XY scanner, the beam is again expanded with a lens system to fill the aperture of the lens, which focuses the radiation on the sample. The generated nonlinear signal can be detected both in the "epi" and "trans-" configuration of the microscope; for this purpose, a dichroic mirror is installed in the optical path of the microscope, cutting off the pump radiation from the useful signal.

Fluorescence lifetime imaging microscopy (FLIM). As mentioned earlier, spectral and temporal characteristics of a fluorescence signal do not depend on the excitation pathway. This allows using the advantages of multiphoton excitation in such a method as fluorescence lifetime imaging microscopy (FLIM).

FLIM is a type of microscopy in which the spatial distribution of fluorophore lifetime is displayed on the image (Fig. 2a) [3]. Visualization of lifetime provides another way of contrasting that, in a first approximation, does not depend on such factors as incident radiation intensity and optical path length, which are difficult to control in biological objects. Fluorescence lifetime depends on internal properties of the fluorophore itself, as well as on its interaction with its immediate environment: for example, in decay kinetics, the effects of dynamic quenching, resonant energy transfer, or changes in the conformation of the fluorophore can be exhibited [3].

A multiphoton microscope can be equipped with FLIM module, e.g., based on time-correlated single photon counting (TCSPC) technique [3]. Other detection

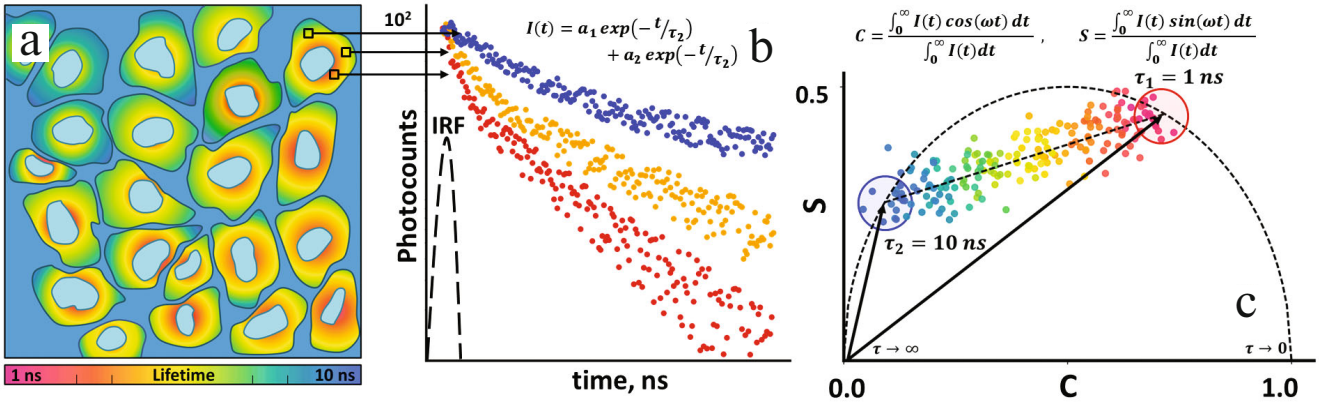

Fig. 2. A schematic representation of: a) cells obtained by the FLIM method: color-coded fluorescence decay time (from fast (1 ns, red) to slow (10 ns, blue); b) fluorescence decay curves for various image points. c) Representation of FLIM data on a phase diagram: each point corresponds to a pixel of the image, with the color-coded fluorescence decay time in accordance with (a).

methods, as well as details related to the FLIM method, are described in detail in the literature [37].

The concept of the TCSPC method can be briefly described as follows. A pulsed radiation source excites the molecules of the substance under study, after which a detector determines the time elapsed between the excitation radiation pulse and a fluorescence photon emitted by the sample. The detected intensity of the fluorescence signal undergoes attenuation in order to detect single photon per excitation pulse. In this case, with numerous repetitions, a histogram of time counts will represent the dependence of the fluorescence signal intensity over time.

After excitation, the dependence of the fluorescence signal intensity on time, $F(t)$, has the shape of an exponential curve:

$$F(t) = A \cdot \exp\left(-\frac{t}{\tau}\right), \quad t > 0, \tag{5}$$

where τ – fluorescence decay time; A – signal intensity at the initial time (amplitude), proportional to the quantum yield of fluorescence and the total concentration of the fluorophore. If several different fluorophores are present in the sample, the time signal will be the sum of the exponentials:

$$F(t) = \sum_i a_i \exp\left(-\frac{t}{\tau_i}\right), \quad t > 0, \tag{6}$$

where a_i and τ_i – amplitude and characteristic decay time of the i-th fluorophore (Fig. 2b). However, such dependence is valid only in the case of an ideal detector that instantly responds to input and absence of any additional noises. In fact, the detected signal $S(t)$ is a convolution of the fluorescence signal $F(t)$ with the response function of the detector's IRF(t) (Instrument Response Function):

$$S(t) \propto \int_0^t IRF(t') \cdot F(t - t')dt'. \tag{7}$$

The FLIM data processing methods can be divided into parametric and non-parametric ones. In parametric approaches, the detected time signal is approximated by a function, the form of which is defined and determined by certain parameters. For example, the decay law is assumed to be two-exponential and parameters a_1, τ_1, a_2, τ_2 are chosen so that the signal convolution (Eq. (6)) reflects the experimental signal most accurately. For instance, in the least squares method, the approximation function and experimental points are compared by the weighted standard deviation.

Thus, fluorescence decay parameters can be determined for each pixel of an image independently of other pixels. It is often assumed that there are at least two chromophores in a sample, and two exponents are used for FLIM approximation (see Eq. (5)), and after that, the mean lifetime, τ_m, is visualized on the image (Fig. 2a):

$$\tau_m = \frac{a_1\tau_1 + a_2\tau_2}{a_1 + a_2}. \tag{8}$$

The disadvantage of "pixel-by-pixel" processing of FLIM images is the need for a large number of photocounts for approximation. If restoring one decay time and one amplitude of a monoexponential curve requires about 200 photocounts, then reliable determination of two lifetimes requires at least 10,000 photocounts [38]. The accumulation of such a number of photocounts in the kinetics for each pixel of an image significantly increases the image acquisition time and may also lead to a photodegradation of the sample – usually, the number of counts for one kinetics does not exceed several thousands.

In non-parametric methods, no approximation of the time signal by a known function is required – instead, values characterizing the fluorophore ensemble are calculated directly from the experimentally measured time signal. These methods allow to conveniently visualize temporal characteristics, while taking significantly less time to process FLIM data [39-41].

For instance, the phasor plot method has been widely adopted recently [39]. In this approach, the time signal is convoluted with sine and cosine functions:

$$C = \frac{\int_0^\infty I(t)\cos(\omega t)dt}{\int_0^\infty I(t)dt}, \; S = \frac{\int_0^\infty I(t)\sin(\omega t)dt}{\int_0^\infty I(t)dt}, \tag{9}$$

where $I(t)$ – the dependence of the fluorescence signal on time, ω – the frequency that in [39] was suggested to be chosen inversely to detection time interval. In fact, such a transformation is similar to isolation of Fourier amplitude of the time signal on frequency ω. For a monoexponential curve with a characteristic decay time τ, the C and S values are provided by the equations:

$$C = \frac{1}{1+(\omega\tau)^2}, \; S = \frac{\omega\tau}{1+(\omega\tau)^2}. \tag{10}$$

If we now mark this point on the C–S plane, then this point will be located on a semicircle with a unit radius and a center at (0.5; 0) (Fig. 2c). If the time signal is a sum of several exponents, C and S values will be superpositions of the following type:

$$C = \sum_i \frac{f_i}{1+(\omega\tau_i)^2}, \; S = \sum_i \frac{f_i\omega\tau_i}{1+(\omega\tau_i)^2}, \tag{11}$$

where

$$f_i = \frac{a_i\tau_i}{\sum_j a_j\tau_j}$$

is relative contribution of the i-th fluorophore to mean fluorescence intensity. For instance, if fluorescence decay kinetics is biexponential, then the corresponding point on the phase diagram will be located on the segment connecting the points corresponding to monoexponential decays with times τ_1 and τ_2. Proximity to each of the points will be determined by the relative contributions of

the first and second fluorophores. Basically, the vector addition rule works on the *C–S* plane (Fig. 2c). The convenience of the phasor plot method also involves the fact that it is possible to simultaneously visualize a large number of fluorophores according to their temporal characteristics [42, 43], which will be illustrated in section "Several Applications of MPM for Studying Biochemical Processes in Connective Tissue and Biomedical Diagnostics".

THE ORIGIN OF ENDOGENOUS REPORTER MOLECULES IN MPM: SOURCES OF MULTIPHOTON AUTOFLUORESCENCE AND OPTICAL HARMONICS

Tryptophan and tryptophan-containing proteins. Intrinsic fluorescence of protein macromolecules, caused by the presence of aromatic amino acid residues (Trp, Tyr, Phe), is widely used for studying conformational changes, intermolecular interactions, biochemical processes in the cell, and for biomedical diagnostics [13]. Fluorescence of tryptophan residues is the most intense, while fluorescence of tyrosine residues in tryptophan-containing proteins is quenched [44], and in the field of molecular imaging, intrinsic fluorescence of proteins usually stands for tryptophan fluorescence. Fluorescence intensity, the shape of the fluorescence spectrum, and relaxation kinetics of the excited state of tryptophan are widely used not only for experiments *in vitro*, but also in fluorescent biomedical diagnostics [13, 14].

Being a classical fluorophore at single-photon excitation, tryptophan is much less often used as an informative signal source in multiphoton microscopy. This fact is primarily due to the absence of an optimal pump wavelength (~600 nm) for TP excitation of Trp (the maximum single-photon absorption of which is in the 280 nm region, and the emission maximum – in the 310-360 nm region, depending on the environment [13] (see table)) in most of the laser sources used in MPM, as well as the lesser depth from which the Trp fluorescence signal can be detected compared to other fluorophores. In addition, measuring such an informative parameter of tryptophan fluorescence as its spectrum shape is hardly possible in

Photophysical parameters of endogenous fluorophores: λ_{ex}, excitation wavelength; λ_{em}, position of emission spectrum maximum; τ, mean lifetime of an excited state. Indices 1PE, 2PE, 3PE refer to single-, two- and tree-photon excitation, respectively

Fluorophore	λ_{ex}, nm	λ_{em}, nm	τ, ns
Tryptophan	$280^{(1PE)}$ $600^{(2PE)}$ [46] $760^{(3PE)}$ [47, 48]	310-360 [50]*	0.1-10*
Serotonin	$760^{(3PE)}$ [49]	340 [49]	–
Collagen	$760^{(2PE)}$ [51]	370-440 [52]	1 [51]
Elastin	$760^{(2PE)}$ [51]	475 [53]	1.3 [51]
Keratin	$350^{(1PE)}$ [54] 700-$900^{(2PE)}$ [55] 764 [53]	420 [54] 450-520 [55]** 465 [53]	–
Fluorescent glycation products (AGEs)	$350^{(1PE)}$ [56] $760^{(2PE)}$ [57]	$450^{(1PE)}$ [56]	–
$NAD(P)H^F$	330-$360^{(1PE)}$ [10] <$760^{(2PE)}$ [58, 59]	460 [60]	0.4 [61]
$NAD(P)H^B$	330-$360^{(1PE)}$ [10] <$760^{(2PE)}$ [58, 59]	440 [60]	1-6.5 [61]*
FAD^F	360, $450^{(1PE)}$ [62] 725-760, 850-$950^{(2PE)}$ [59]	50 [59]	2.3-2.9 [10]
Melanin	760-$800^{(2PE)}$ [63]	550 [63, 64]	0.1 [63]
Lipofuscin	400-$500^{(1PE)}$ [12] 755, $860^{(2PE)}$ [65]	480-700 [12]	0.4 [66]

* Depending on the environment.
** Depending on the excitation wavelength.

microscopy experiments. This is due to the fact that for most of the used setups, detection is carried out at fixed wavelengths without spectral resolution.

The number of studies on MPM with Trp fluorescence signal is rather limited; however, the available results allow us to estimate the prospects of further using this signal in MPM. For example, in [45] MPM was used for rat skin *in vivo*, achieving an increased contrast in visualization of dermis cells in comparison with the signal from other fluorophores, NAD(P)H and FAD. This is due to the localization of the signal from the latter in small areas (predominantly in mitochondria), while Trp fluorescence is distributed over a cell evenly. MPM using Trp AF also allows the detection of leukocytes *in vivo* [46].

AF of Trp can also be obtained by three-photon excitation (λ_{ex} ~ 700-800/λ_{em} ~ 350 nm), and the low absorption cross section can be compensated for by a high fluorophore concentration. Thus, Trp AF with three-photon excitation was used for metabolic imaging together with signals from NAD(P)H and FAD [47, 48] – this aspect will be discussed in the section "MI with Trp fluorescence as an indicator". Also of interest is the detection of tryptophan metabolites, in particular, of serotonin, using MPM [49], for which three-photon excitation is used [31].

Fluorescence of structural proteins of connective tissue and epidermis. A number of fibrillar proteins, which are the main components of tissue – collagen, elastin, and keratin – emit fluorescence with a maximum in the 450 nm region when excited in the 350 nm region [54, 67]. This fact is due to the presence of so-called crosslinks in their structure [68]. Nevertheless, the chemical structure and optical properties may differ for elastin [69], collagen [70], and keratin [71]. AF of structural proteins is considered in detail in the context of the tasks of biomedical diagnostics, in particular, skin studies [67, 72]. Collagen is the most common protein in the human body. Collagens of various types, as well as collagens obtained from various sources, have varying spectral properties and fluorescence lifetimes [73]. The data on the absolute values of the lifetimes of the excited state of collagens of various types and elastin vary significantly [51].

Keratin in the skin is synthesized by keratinocytes, cells that make up 90% of the epidermis. Over time, keratinocytes move from the basement membrane to the surface of the skin while synthesizing more keratin. Therefore, the highest concentration of keratin is detected in the *stratum corneum* of the skin, which consists of dead cells – corneocytes [74]. The *stratum corneum* exhibits intense fluorescence and, despite its rather small thickness compared with penetration depth of excitation radiation, makes a significant contribution to the AF spectra of skin [72]. The optical properties of keratin under TP excitation in the region of 700-900 nm were analyzed in [55]. The shape of the fluorescence spectrum of a keratin sample was shown to depend on excitation wavelength, shifting to the long wavelength region with increasing pump wavelength (the position of the maximum shifts from 450 to 500 nm with an increase in the excitation wavelength from 760 to 900 nm), which is probably due to excitation of various groups of fluorescent crosslinks.

Fluorescence of proteins caused by biochemical processes: glycation and oxidation. A number of biochemical processes can also affect the optical properties of structural proteins. For example, during glycation of protein molecules, fluorescent endproducts of glycation can form (AGEs, advanced glycation endproducts) [75, 76], in particular, pentosidine [77]. In diabetes, darkening of skin is observed due to collagen glycation [78], and the fluorescent signal from the resulting glycation products is widely used to diagnose the disease and quantify the degree of glycation of structural proteins [56, 75]. Excitation of AGE fluorescence is usually carried out at 350 nm, and their emission spectrum is broad with a maximum in the region of 450 nm and similar to AF spectra of structural proteins [56]. The glycation process also vividly manifests in optical properties of the tissue under TP excitation. For example, in [57], glycation of *ex vivo* skin samples was analyzed by MPM. AF intensity was shown to increase with glycation of collagen, while the intensity of the SHG signal decreases. Similar results were obtained in *in vitro* experiments on collagen glycation [79], as well as *ex vivo* for various connective tissue samples [80]. This fact is a consequence of the formation of fluorescent AGEs, resulting in an increase in AF, and a disruption in collagen structure, leading to a decrease in SHG.

Oxidation processes can also significantly affect the fluorescent properties of structural proteins, primarily due to their effect on aromatic amino acid residues [71, 81-83]. The processes of aging and the related accumulation of reactive oxygen species (ROS) can also cause post-translational modifications of proteins and formation of new fluorescent crosslinks [84].

In terms of the origin of endogenous fluorophores, the fact that "blue" fluorescence – virtually similar in its spectral properties to the fluorescence of structural proteins – can be observed in globular proteins is important as well [85]. In a number of papers [86-88], blue fluorescence of globular proteins is used as an aggregation marker (in particular, of fibrillation), and the nature of the fluorophore responsible for it is debatable [89]. In [90], it was demonstrated that blue fluorescence can be observed not only for aggregates, but also for monomers of globular proteins and is linked to the presence of carbonyl groups in them. Finally, blue fluorescence can also be observed during oxidation and glycation of monomers of globular proteins [91].

Thus, the characteristic signal of connective tissue emission with a maximum in the 450 nm range with single-photon excitation in the range of near UV and TP

excitation in the range of 700-800 nm can be associated with both fluorescent crosslinks in structural proteins and posttranslational modifications of fibrillar and globular proteins. Although this signal is not specific for fluorophores of the same type, it can be used for biomedical diagnostics if there is a priori information about the object [88].

Nicotinamide adenine dinucleotide (NADH) and nicotinamide adenine dinucleotide phosphate (NADPH). NAD and NADP are universal cofactors involved in a multitude of redox processes in cells of living organisms [92]. These molecules are apparently the most frequently used endogenous markers in conducting research on living objects using methods of fluorescence spectroscopy in general and MPM in particular.

The redox state of the cell is a determining factor in bioenergetic processes and metabolism and is directly related to pathological processes in the body. Oxidized and reduced NAD and NADP play an important role in the redox state of the cell, being involved in a number of key metabolic processes. NAD is responsible for ATP production in the cytoplasm by glycolysis and in mitochondria by oxidative phosphorylation (OP), and NADP is involved in biosynthesis of lipids, amino acids, nucleotides, and protection against ROS. Therefore, the generation of ROS depends on the redox state of NAD, while NADP acts as an antioxidant protection of the cell [61].

The nicotinamide fragment of NADH absorbs in the range of 340 ± 30 nm and emits fluorescence in the range of 460 ± 50 nm, while the spectral properties of NADPH are similar due to the remoteness of the phosphate group from the nicotinamide fragment, which is the chromophore and fluorophore of NAD(P)H [9]. In this regard, NAD(P)H is the designation usually used in literature as the name of the fluorophore, since precise identification of the source of fluorescence is difficult. At the same time, oxidized forms of $NAD(P)^+$ do not possess the indicated absorption bands and, accordingly, fluorescence, which makes it possible to determine the NAD(P)H/$NAD(P)^+$ ratio – redox status of the cell – by using fluorescence spectroscopy with single-photon excitation in the region of 360 nm or with TP excitation in the region of 700-800 nm [93]. In addition to fluorescence intensity, another approach to analyzing metabolic processes is widely covered in the literature, which is based on measurements of NAD(P)H fluorescence decay kinetics (see also section "Several Applications of MPM for Studying Biochemical Processes in Connective Tissue and Biomedical Diagnostics").

Since NAD(P) is a cofactor in a number of catalytic reactions, and its optical properties (in particular, the lifetime of the excited state) are sensitive to microenvironment, time-resolved fluorimetry allows analysis of the biochemical processes involving them. The fluorescence lifetime of free NAD(P)H in a solution varies in the range of 0.3-0.8 ns, whereas for the form bound to an enzyme, it increases to 1.0-6.5 ns, depending on the protein [61]. Fluorescence relaxation kinetics of NAD(P)H is usually interpreted as follows: for a biexponential approximation, the first (fast) time is assigned to the free form, $NAD(P)H^F$, and the second (slow) time – to the bound form, $NAD(P)H^B$: hereinafter, superscripts F ("Free") and B ("Bound") will denote the free and bound forms, respectively. It is known that due to NAD(P) being a cofactor for various enzymes, the measured relaxation kinetics is averaged over a heterogeneous system of fluorophores with different lifetimes. Despite the high demand for this approach and its productivity in studies of biochemical processes, the interpretation of the relaxation kinetics of the excited state of NAD(P)H in a cell is still a matter of discussion [58, 60, 94].

$NAD(P)H^F$ exists in two conformations in a solution, folded and unfolded, that are in dynamic equilibrium. The relaxation kinetics of $NAD(P)H^F$ AF consists of two components with times that are approximately 0.2 and 0.6 ns, and their spectral properties are identical [60]. The longer lifetime corresponds to the folded conformation, which was explained in [95] by formation of an exciplex (a complex with charge transfer formed in the excited state) during the interaction of nicotinamide and adenine fragments. Nevertheless, a number of other hypotheses appeared later in the literature, explaining the biexponential character of the relaxation kinetics of $NAD(P)H^F$ by various photophysical processes in the nicotinamide fragment of the molecule [96]. The increase in the lifetime of NAD(P)H upon its binding to enzymes is determined by the conformation of the cofactor at the binding site and the restriction of its mobility [96].

In a number of studies, it is pointed out that $NAD(P)H^B$ can also contribute to the fast component of relaxation kinetics [60, 94]. Moreover, a decrease in the mean fluorescence lifetime of NAD(P)H in a cell can be due to a redistribution of contributions from $NAD(P)H^B$ associated with various enzymes, rather than to an increase in the $NAD(P)H^F$/$NAD(P)H^B$ ratio [94]. Further, in study [58], it was shown that contribution of NADPH to NAD(P)H fluorescence kinetics in cells is very significant. Using the methods of molecular biology and applying a number of substances to affect the NAD/NADP ratio in a cell, the authors demonstrated that after excitation at 700 nm, the lifetimes of $NADH^B$ and $NADPH^B$ in cells were 1.5 ± 0.2 and 4.4 ± 0.2 ns, respectively. The main conclusion was that changes in fluorescence decay kinetics of NADPH in a cell cannot explicitly indicate a change in metabolism from OP to glycolysis, since they may be associated with the redistribution of the contributions of NADH and NADPH to the kinetics during metabolic changes.

To summarize, fluorescence intensity and relaxation kinetics of NAD(P)H are informative indicators for studying biochemical processes in cells, primarily those

related to metabolism, some examples of which are given in section "Several Applications of MPM for Studying Biochemical Processes in Connective Tissue and Biomedical Diagnostics". At the same time, a detailed analysis of photophysical processes with their participation in cells is still a priority [58, 61]. One of the approaches providing additional information about cell redox state is simultaneous measurement of signals from NAD(P)H and flavin adenine dinucleotide, FAD, which is a "complementary" cofactor-indicator of the metabolic cell state [97].

Flavin adenine dinucleotide (FAD) and riboflavin. In cells, FAD is mainly a cofactor for enzymes involved in redox processes [59, 98]. The number of flavoproteins (FP) is very large, but for most of them, flavin fluorescence of cofactors is quenched due to electron transfer to them from aromatic amino acid residues [99]. Additionally, the conformation of FAD plays a decisive role during its binding – in the presence of interaction between two FAD fragments (stacking), the lifetime and quantum yield of fluorescence decrease [62]. A detailed analysis of the photophysical properties of FAD and FP can be found in [62].

It is known that two FPs involved in metabolic processes (lipoamide dehydrogenase and electron transfer FP) make a major contribution to FAD fluorescence [59, 98]. Due to the fact that only FPs with an oxidized cofactor and only the reduced form of NAD(P)H are fluorescent, the corresponding signals react to a change in the metabolic state in reverse [59, 98]. In this regard, determining the cell redox state by measuring the ratio of NAD(P)H and FAD signals is widely used to monitor the metabolism of cells and tissues, and this includes using MPM [59, 97]. The redox ratio can be calculated from the fluorescence intensities of NAD(P)H and FAD in several ways [100], but in any case, this parameter is not affected by artifacts associated with measuring absolute intensity values. In contrast to that of NAD(P)H, the fluorescent signal of FAD in MPM can be obtained with a longer excitation wavelength (~850 nm), is less susceptible to photodegradation, and is localized mainly in mitochondria [59].

Besides FAD, riboflavin, a water-soluble vitamin precursor of FAD in cells, is of interest for AF. The results associated with the detection of a characteristic AF signal (λ_{ex} ~ 480/λ_{em} ~ 530 nm) in cancer stem cells (SC) are presented in [101]. The appearance of AF was found to be ATP-dependent, and it was also shown that the ATP-dependent transport protein ABCG2, for which riboflavin is a substrate, is overexpressed in cells with AF and colocalized with membranes of vesicles that exhibit AF within cells. Thus, it was reliably demonstrated that riboflavin is a source of AF specific for cancer SCs.

Melanin. Melanins are heterogeneous pigments responsible for photoprotection and color of skin, hair, and eyes. There are a number of model structures of melanin in the literature, but in general they can be described as heterogeneous polymers resulting from oxidation of phenols and subsequent polymerization of intermediate phenols and quinones formed from them [102].

The spectrum of single-photon melanin absorption in the visible and near-IR spectrum regions is well described by an exponent decreasing with the wavelength. With single photon excitation, melanin AF is in the 400-700 nm region, and its intensity is low compared to other connective tissue fluorophores (for example, NADH and FAD). Melanin is also able to fluoresce with single photon IR excitation (λ_{ec} ~ 785/λ_{em} ~ 820-920 nm) [103].

When melanin is excited by short pulses in the infrared range, intense fluorescence is observed. According to [64], the process of absorption of two photons by melanin is two-step and not two-photon, that is, it occurs in two stages with the participation of an intermediate real electronic state. This is due to the fact that, unlike other fluorophores, melanin has a significant absorption cross section in the infrared region of the spectrum, and since the lifetime of its excited state is short (~100 ps), a large photon flux density is required for absorption from the excited state to occur, which happens when using a laser radiation source with parameters characteristic of MPM. This being said, the two-step absorption cross section of melanin is larger than TP absorption cross sections of most fluorophores in connective tissue, making it possible to carry out selective melanin imaging, which underlies studies on diagnosing pathological processes in skin [63, 104]. Another parameter that allows isolation of the contribution of melanin AF is its short fluorescence lifetime (~200 ps) [63].

Lipofuscin. Another endogenous fluorophore, localized mainly in cell lysosomes, is lipofuscin, which is a heterogeneous formation consisting of proteins, lipids, and/or carotenoids, distinguished by the presence of crosslinks and its oxidation [105]. Lipofuscin formation is often associated with pathological processes in the body, such as oxidative stress and aging, both of which are associated with the accumulation of degradation products in cells. Lipofuscin is believed to be a pigment of aging, and therefore it is often regarded as a marker of pathological processes [106].

Due to heterogeneity of its molecular composition, the optical properties of lipofuscin are characterized by wide spectral ranges of fluorescence excitation (300-500 nm) and emission (480-700 nm) [107]. A detailed analysis of the spectral properties of lipofuscin is complicated by the fact that its optical properties largely depend on its concentration: in the case of dense packing of molecules in granules, the effect of the internal filter should be taken into account, i.e., self-absorption of fluorescence by lipofuscin, resulting in a shift of the emission maximum to the long-wavelength region (the so-called metachromic effect [108]). The simultaneous detection

of signals from lipofuscin, NAD(P)H, and FAD is a promising tool for analyzing pathological processes and oxidative stress by MPM (for more details, see section "Several Applications of MPM for Studying Biochemical Processes in Connective Tissue and Biomedical Diagnostics").

In histological studies, AF resulting from the presence of lipofuscin appears to be a problem: due to the considerable width of the spectra of fluorescence excitation and emission, the signal from lipofuscin can mask even an intense immunofluorescence signal. To counter this phenomenon, tissue samples are dyed with Sudan Black dye, which is an effective fluorescence quencher [109]. Also, in [66], a method was proposed for isolating the signal of a fluorescent probe embedded in amyloid bodies from the background lipofuscin signal for MPM *in vivo*. The proposed approach relies on both the spectral features of lipofuscin and the short lifetime of its fluorescence (~0.4 ns) compared to the probe.

In addition to the radiation of the lipids contained in lipofuscin, an emission from oxidized lipids that are not localized in granules can be observed. In [53], by using MPM and spectral detection, it was shown that fluorescence of stratum corneum, as well as of intercellular space of the upper skin layers, is shifted to the long-wavelength region compared to keratin and NAD(P)H spectra and, at least partially, is associated with lipids.

Optical harmonic generation. The SHG signal associated with the response of type I collagens (in the dermis) carries information on its concentration, morphology, and localization, which is important for clinical studies. A review of SHG applications for molecular imaging, including that of collagen fibers, can be found in the book [15]. Images of extracellular matrix obtained by SHG usually contain filamentary structures, and a number of methods are used in the literature to analyze such images. The most common method is based on the Fourier transformation of the image, in the literature this is referred to as FT-SHG. The method is based on the fact that a two-dimensional Fourier transformation spectrum contains information on the prevalent directions in the image [110]. The Fourier transformation frequencies are inversely proportional to the dimensions of the spatial features, and the maximum frequency of the Fourier transformation corresponds to the minimum characteristic size of the image. In general, it can be argued that SHG microscopy is one of the most relevant modalities of MPM and allows extraction of valuable information on the organization of extracellular matrix [110].

The MPM method allows simultaneous measurements of type I collagen distribution (by SHG intensity) and elastin distribution (by AF) in real time *in vivo* [1]. The most promising approach to imaging structural proteins in connective tissue is considered to be multimodal detection, when AF, SHG, and FLIM signals are simultaneously measured [43, 51]. SHG microscopy may also be convenient for studying nanoparticles. In particular, in [111], the depth of zinc oxide nanoparticle penetration into the epidermis was determined using SHG.

The third harmonic generation effect (THG) provides an additional contrasting mechanism, which in this case can be combined with other types of nonlinear optical microscopy [15, 112, 113]. As mentioned earlier, unlike SHG, no specific spatial arrangement or asymmetry of substance molecules is required for a response on the tripled frequency – it can be generated by any environment. However, with THG microscopy, a signal is usually not observed from homogeneous environments due to a destructive wave interference in a converging beam of excitation radiation [17]. In this regard, contrast THG images are obtained if optical inhomogeneities are comparable to the focal spot in size. For example, lipid droplets [112] and lipid-accumulating organelles, the size of which is several hundreds of nanometers [114], can be visualized this way. An overview of the use of THG is given in [113]: THG microscopy allows visualizing the cell membrane, nuclear morphology, hemodynamic studies *in vivo*, separation of leukocyte types, etc. It is important to note that the detection of AF, THG, and SHG can be carried out in MPM simultaneously by detecting the signal in different spectral channels [115], thus ensuring multimodality.

SEVERAL APPLICATIONS OF MPM FOR STUDYING BIOCHEMICAL PROCESSES IN CONNECTIVE TISSUE AND BIOMEDICAL DIAGNOSTICS

Studies of cell metabolism with the use of fluorescence of cofactors NAD(P)H and FAD began with the works by B. Chance in the 1960s and became very popular in various fields of research. The development of optical microscopy methods, in particular, confocal microscopy, allowed metabolic imaging (MI)[1] – analysis of redox status of a cell, determined through the parameters of NAD(P)H and/or FAD fluorescence signal – with subcellular spatial resolution, and introduction of the FLIM method in the 1990s led to the appearance of an additional information channel based on measuring fluorescence decay kinetics, which was free from the shortcomings of the approach based on measuring signal intensity [116].

Finally, the development of MPM allowed to perform MI on 3D structures with a smaller contribution of photodegradation. Over the years of its existence, using MI accumulated a large body of data in various fields, which has been reflected in a number of reviews – for

[1] Henceforth, metabolic imaging refers to fluorescent metabolic imaging in which only the fluorescent fraction of the cell metabolome is tracked.

example [9, 10, 61]. In view of this, we briefly describe the major results and trends in MI with MPM-FLIM in this review and elaborate on its less conventional applications with the focus on photophysical processes underlying the observed changes in the signal from cells, as well as on using endogenous fluorophores in addition to NAD(P)H and FAD.

Studies of oncological processes. Cancer cell research in 2D and 3D models with using MPM-FLIM is aimed both at studying fundamental aspects related to their metabolic features and heterogeneity, and at developing methods for diagnosing tumor cell response to anticancer drugs. Additionally, the possibility of clinical use of MI for biomedical diagnosis of cancer and navigation through a surgical field is discussed extensively in the literature [2]. Due to the fact that a number of reviews [9, 10, 100, 117] are devoted to this area of research, we are not delving into any specific examples in this work, but considering only the general picture which reveals the general idea of the mechanisms underlying changes in fluorescent properties of NAD(P) and FAD in oncological processes, although we do not claim it to be a complete description of them.

Numerous studies of cancer cells with using MI demonstrate a decrease in the redox status of such cells and a decrease in the mean lifetime associated with an increase in the share of $NAD(P)H^F$. These results are often interpreted on the basis of the Warburg hypothesis, suggesting a change in the metabolism of cancer cells from OP to glycolysis even under normal conditions of oxygenation, caused by irreversible mitochondrial dysfunction [118]. Although it is currently established that the Warburg hypothesis is not generally correct and only certain tumor lines have mitochondrial dysfunctions, and inhibition of glycolytic processes results in a reverse transition of tumor cells to OP, the trend of switching to glycolytic metabolism exists [100, 118, 119].

In general, most reports characterize cancer cells by a smaller FAD/NADH ratio (and increased NADH fluorescence) and a shorter NADH lifetime compared to the norm, whereas a reverse trend is observed when tumor cells are treated with anti-cancer drugs [10, 117]. The first observation is primarily related to the fact that NADH accumulates during glycolysis, whereas during OP, it is oxidized to NAD^+ in mitochondria, and the reverse process is observed for FAD. The second observation is due to the fact that the free form of NADH is localized predominantly in cytosol and is involved in glycolysis, while the bound form is involved in OP. This generalization certainly has exceptions, as can be seen, for example, from the compilation of results carried out in the review [10]. The redox status and the ratio of concentrations of free and bound forms of NAD(P)H were demonstrated to allow detecting precancerous cells, distinguishing cells of different degrees of proliferation, investigating the characteristics of response and resistance for different cell lines, etc. [9, 10, 100, 117]. In particular, MI allows a characterization of the response to treatment already at an early stage, which may be used for personalized medicine [117].

Studies of stem cell (SC) differentiation. MI has also been applied to studying the processes associated with SCs, namely, the processes of their differentiation. In addition, of interest is the analysis of cell population heterogeneity for isolation of pure lines and their application in cell therapy. It should be noted that analysis of MPM-FLIM data – based on representation of fluorescence decay kinetics with a phase diagram – has become wide-

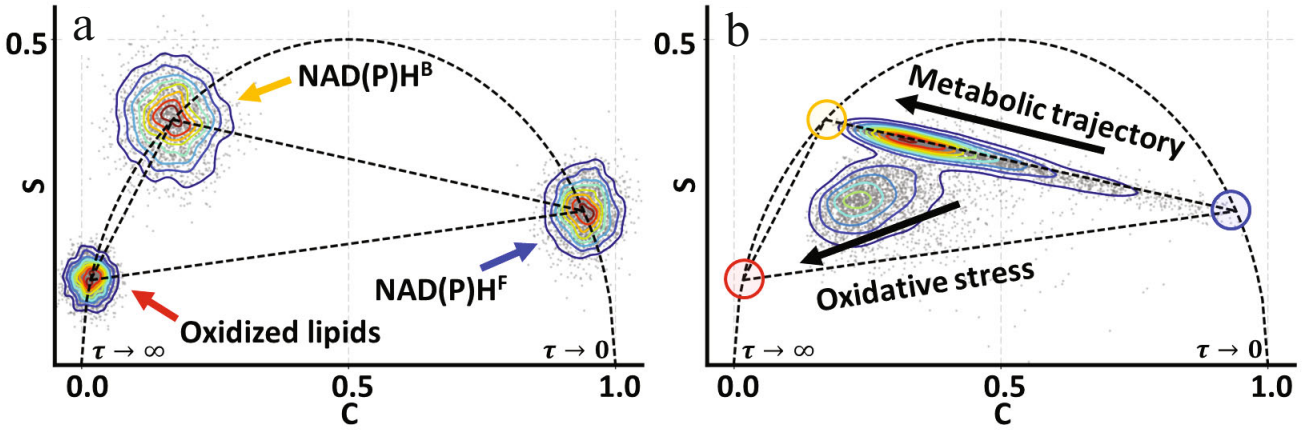

Fig. 3. A schematic representation of FLIM data on a phase diagram. a) Pixel distribution in a model FLIM image corresponding to $NAD(P)H^F$ ($\tau \approx 0.4$ ns), $NAD(P)H^B$ ($\tau \approx 3$ ns) and oxidized lipids ($\tau \approx 7.5$ ns) on a phase diagram; level lines illustrate pixel distribution by signal intensity. b) Pixel distribution in a FLIM image corresponding to the model experiment. The group of pixels located along the segment connecting the areas that correspond to $NAD(P)H^F$ (blue circle) and $NAD(P)H^B$ (yellow circle) corresponds to fluorescence relaxation kinetics of NAD(P)H, where a shift towards $NAD(P)H^F$ corresponds to glycolysis, and towards $NAD(P)H^B$ – to OP. The presence of oxidative stress results in a shift of the group towards oxidized lipids (red circle). Figure 3b is adapted from [120].

spread in this field (see section "The Multiphoton Microscopy Method"). The pixels corresponding to $NAD(P)H^F$ (with a short lifetime) and to $NAD(P)H^B$ are clustered in different parts of the diagram (Fig. 3), and the shift of pixel distribution in the coordinates of the phasor plot may indicate a redistribution of NAD(P)H forms and a change of the main type of metabolism (the so-called metabolic trajectory). Moreover, a number of reports analyze the width of pixel distribution in a diagram and study it with regard to heterogeneity of fluorophores associated with many NAD-dependent enzymes.

The general trend observed in studies of SC differentiation using the MPM-FLIM method is an increase in the mean cell fluorescence lifetime when they are excited in the 700-760 nm region, which is explained by an increase in the fraction of $NAD(P)H^B$. At the same time, a shift from glycolysis to OP on the metabolic trajectory is observed in the following sequence: SCs – progenitor cells – differentiated cells [121]. Moreover, the analysis of data on the phasor plot allows a separation of different cell cultures using clustering methods [122]. This approach allowed, in particular, to distinguish SCs and progenitor nerve cells at different stages of differentiation, despite the fact that these stages were indistinguishable by cell morphology and expression of markers [123].

The authors [124] investigated the differences in the distribution of free and bound forms of NAD(P)H in the L6 myoblast cell line for undifferentiated cells and cells that were in the early stage of differentiation. The most striking difference was shown to lie in a significant increase in the proportion of $NAD(P)H^B$ in cell nuclei of cells at the early stage of differentiation, which was interpreted as a result of the increased activity of transcription processes and chromatin structure in comparison with undifferentiated cells (the so-called increased nucleus activity). Note that this interpretation differs from the widely used concept of "metabolic trajectory", which operates with the parameters of NAD(P)H fluorescence in mitochondria and cytosol (see, for example, the previous section). The interaction of regulatory proteins with NAD in the nucleus is an important factor influencing the process of transcription [125]. Thus, MPM-FLIM theoretically allows non-invasive analysis of the processes occurring in the nucleus, but its application is currently less widespread than that of MI [124, 126]. This is probably due to the low signal from the nucleus region and the complexity of interpreting the data, but this approach undoubtedly reveals qualitative differences between cells.

MPM-FLIM also allows an analysis of SCs *in vivo*. For example, in [127], temporal oscillations of SC metabolic status of epidermis of mice were demonstrated *in vivo*. Using NAD(P)H fluorescent signal, it was shown that the circadian rhythm cyclically coordinates changes in the contributions of glycolysis and OP with the activity of DNA synthesis. The authors demonstrated an increase in the proportion of $NAD(P)H^F$ at night, coinciding with the largest proportion of SCs that are in the S phase of the cell cycle, and suggested that this may be due to the need to maintain low ROS concentration during active proliferation.

Studying oxidative stress. Under normal metabolism, ROS can play a signaling role in the regulation of redox homeostasis in cells. An accumulation of ROS in concentrations exceeding the normal physiological level can result in oxidative stress – DNA damage, oxidation of protein and lipid molecules, which, in turn, may cause a number of pathologies – inflammatory processes, diabetes, cancer, and cardiovascular and neurodegenerative diseases [92]. Oxidative stress and associated increased concentrations of ROS can be detected by a number of methods, including the use of fluorescent probes. At the same time, of interest is the method of studying oxidative stress with endogenous fluorophores, for which signals of NADH, FAD, and oxidized lipids are used.

For example, in study [120], the use of MPM demonstrated that under oxidative stress, lipid droplets are formed in cells, which are characterized by a long lifetime (7.5 ns). By presenting the distribution of fluorophores in a cell by the parameters of decay kinetics on the phasor plot, the authors show that in addition to the "metabolic trajectory" corresponding to redistribution of NAD(P)H between the free and bound forms in a cell, there is an "oxidative stress trajectory" (Fig. 3), characterized by the appearance of a pixel group on the FLIM image that corresponds to the long decay time. A similar approach was used to study oxidative stress in cardiomyocytes during hypoxia and under the action of cardiotoxins [128].

Similar results were obtained in [122] when differentiation of embryonic SCs was studied. It was shown that in undifferentiated embryonic SCs, granules of ~1 μm size are detected ($\lambda_{ex} = 760/\lambda_{em} \sim 500$ nm) that are characterized by slow fluorescence decay (~10 ns). The authors argue that these granules contain lipids and explain this by the fact that in undifferentiated embryonic SCs, their presence is caused by a high concentration of ROS, associated with high OP rate, as well as an excess of unsaturated fatty acids that can form fluorophores during oxidation.

It is important to observe that the authors [120, 122] note that lipofuscin cannot be responsible for the fluorescence of granules with longer lifetimes, referring to the fact that it is characterized by a much faster fluorescence decay and a wide excitation spectrum; in addition, the long-lived signal was not localized in lysosomes [122], as might be expected for lipofuscin [12, 107]. At the same time, in study [65], where adipogenic and osteogenic differentiation of mesenchymal SCs was studied using MPM, it was shown that over time, lipid granules colocalized with lysosomes appear in cells, the fluorescence of which is excited both at 755 and 860 nm. The authors [65]

identify the corresponding fluorophore as lipofuscin and explain its accumulation by oxidative stress in cells. The explanation of the fluorescence of granules by the presence of lipofuscin is also present in [129], where differentiation of embryonic SCs was investigated. In this study, measurements were taken using the excitation wavelength of 366 nm, and the concentrations of fluorophores in cells were measured by factorization of AF spectra into six components (oxidized proteins, $NAD(P)H^F$ and $NAD(P)H^B$, FAD, lipofuscin, and porphyrins). The authors [129] also explain lipofuscin accumulation in SCs by oxidative stress and note a decrease in its levels during differentiation.

To summarize, MPM provides a possibility for noninvasive indirect assessment of oxidative stress by the contribution of lipid granules resulting from oxidation of lipids and ROS proteins to the fluorescence signal. In perspective, this method can be applied not only for studying 2D and 3D cell cultures, but also *in vivo*.

Neurodegenerative diseases. There is a number of evidences in the literature on the fact that mitochondrial dysfunction is one of the key factors in neurodegeneration [130]; however, causal relationships in the development of pathological processes are still not completely clear. Since label-free MPM-FLIM is an informative method for studying the metabolic processes associated with mitochondria, and can also perform molecular imaging, in particular, of proteins and their oligomers [88], its application in studies of neurodegenerative processes in models is of particular interest.

Formation of amyloid fibrils and related bodies is associated with the development of neurodegenerative diseases (Alzheimer's, Parkinson's, and others), in particular, with a deterioration of synaptic connections between neurons [131]. It is also known that predominantly, oligomers of amyloidogenic proteins are toxic. In [132], metabolism of HEK293 cells was analyzed, in which the amyloidogenic protein α-synuclein was overexpressed (HEK293-aS), which is involved in the pathogenesis of Parkinson's disease, as well as that of HEK293-aS cells, with fibrillation seeds (HEK293-seeds) added to their cytoplasm, i.e., mature fibrils, the presence of which greatly accelerates aggregation process. Using MPM-FLIM, it was demonstrated that in the HEK293-aS model, the fraction of the bound form of NAD(P)H increases significantly, which was explained by the incorporation of α-synuclein oligomers into mitochondria and the associated disruption of their functioning and oxidative stress. NAD(P)H was also found to be able to incorporate into mature fibrils that were present in the HEK293-seeds model, further confirmed by experiments *in vitro*. Nevertheless, since according to the authors' estimate, concentration of α-synuclein in the analyzed models was approximately 1 μM, and concentration of NAD(P)H was about 1 mM, the effect of increasing the lifetime of NAD(P)H in HEK293-seeds should be associated with its incorporation into fibrils only to a small degree. The authors [132] suggested that a smaller change in the redox status of HEK293-seeds compared to HEK293-aS is due to the fact that in them, the whole protein was involved in the formation of mature fibrils, and therefore the effect of oligomers on mitochondrial function was smaller.

In [133], metabolic status of differentiated neurons was studied by the MPM-FLIM method. The authors note that this model is more appropriate for Parkinson's disease than the one used in [132]. In the experiment, a decrease in the mean lifetime was observed for NAD(P)H and FAD in the model of Parkinson's disease [134], and the fractions of $NAD(P)H^F$ and FAD^B increased. The authors explained this fact by inhibition of the electron transport chain and concluded that metabolism switches from OP to glycolysis in Parkinson's disease model cells.

Then, the authors [135] studied metabolism in HEK293 cells transfected with plasmids containing exon 1 of the *HTT* gene with a different number of repeats of triplet CAG. This codon encodes the amino acid glutamine, and if the number of its residues in the HTT protein exceeds 40, Huntington's disease develops, while the number of repeats under 36 is the norm. The authors demonstrated that for a larger number of repeats (97 vs 25), a significant increase in the fraction of $NAD(P)H^F$ in cells, including nuclei, was observed, which may indicate translational dysregulation. Similar results were obtained *in vivo* on optic disc cells of transgenic drosophila [135], which are an adequate model for studying neurodegenerative diseases, in particular, Huntington's disease [136], since fruit flies possess a nervous system with specialized functions. Thus, MPM allows study of metabolic processes in neurodegenerative diseases on both *in vitro* and *in vivo* models.

MI with Trp fluorescence as an indicator. In addition to the standard approach to determining the metabolic status of a cell, based on measuring the parameters of NAD(P)H and FAD fluorescence, there are reports in which tryptophan fluorescence serves as an indicator. This method is based on the fact that during the binding of a cofactor (NAD(P)H) by an enzyme, energy is transferred to it from tryptophan residues within the protein by the Förster mechanism with the effective radius of ~2.3 nm [48]. Therefore, the lifetime of tryptophan fluorescence of a cell decreases with an increase in the fraction of the bound form of NAD(P)H. In the studies [47, 48], a simultaneous detection was carried out for Trp AF caused by three-photon excitation and TP NAD(P)H with excitation at 740 nm. The efficiency of the Trp-NAD(P)H energy transfer was demonstrated to correlate with the share of the bound form of NAD(P)H in mitochondria [48] and with the ratio of shares of $NAD(P)H^B$ and FAD^F, which the authors [47] used as indicators of the cell redox state.

Application for skin diagnostics: optical biopsy. Nonlinear optical microscopy is a convenient tool for biomedical imaging due to the physical principles underlying the creation of contrast between individual objects. One of its major advantages is the possibility of reconstructing a three-dimensional image, which, in particular, makes it possible to perform morphological studies *ex vivo* (on biopsy samples) and *in vivo*. In particular, in our study [137], the MPM method was used for non-invasive optical histology of the nail bed – an area studied by the optical capillaroscopy method. The application of MPM established at the cellular level the causes of the correlation of parameters measured by capillaroscopy with the severity of heart failure in patients: it was demonstrated that an edematous syndrome manifests itself as an increase in the size of the perivascular region associated with fluid accumulation in the epidermis. This example illustrates the advantages of MPM in comparison to other methods of optical biopsy that allow histological studies in humans *in vivo*: high spatial resolution and greater (compared to confocal laser microscopy) scanning depth. The main advantage is the ability to analyze the molecular components of connective tissue with simultaneous use of several modalities: AF, SHG, FLIM [1, 43, 51].

In one study [138], the MPM method was used to analyze the morphology of keratinocytes in the presence of skin inflammation processes *in vivo*, and redistribution of mitochondria inside the cells was demonstrated, namely their localization near the nucleus during inflammation. The degree of increase in the mean intercellular distance and decrease in the thickness of epidermis also correlated with the activity of inflammatory processes. A non-invasive morphometric approach to analyzing the distribution of mitochondria in epidermal cells *in vivo* was also applied in [139] to studying oncological diseases. The authors showed that in healthy skin, a gradual change in the distribution of mitochondria in cells occurs with an increase in depth, whereas no such trend exists for tumor tissue, which can be used for diagnostic purposes. Analysis of cell morphology in granular, spinous, and basal layers revealed differences between healthy skin, squamous cell carcinoma, and premalignant keratosis using MPM *in vivo* [140]. Important results were obtained in [141], where cell morphology of the granular layer of the skin (*stratum granulosum*) was studied in order to explain its spatial architecture, which allows maintenance of the so-called tight junctions between cells during their renewal and to insure the barrier function of skin. It was shown that epidermal cells that are responsible for the formation of tight junctions have the shape of a flattened tetrakaidekahedron, and the dynamics of cell transition between layers was visualized, revealing the role cell shape in maintaining the tight packaging and protective properties of the skin. Another example of a non-invasive morphometric study possible using MPM is determining the form of the dermo-epidermal transition (DET), which is, in essence, the shape of papillary dermis surface, which is an indicator of skin aging processes [142]. The visualization of DET is possible due to, first, a significant difference in the optical properties of cells at the basement membrane, namely, to an increased melanin content [104], and second, the presence of SHG signal from type I collagen molecules in dermis [15]. Therefore, the appearance of the SHG signal marks the beginning of DET, and the value of the SHG signal maximum determines the lower boundary of papillary dermis, allowing measurement of its thickness *in vivo* [143]. The use of the MPM-FLIM method also allows *in vivo* visualizing blood vessels in the dermis using red blood cell fluorescence [51]. Due to ultrafast (~30 fs) charge transfer from the porphyrin rings within the heme to the empty d orbitals of the iron ion, hemoglobin is non-fluorescent. Nevertheless, the studies carried out by the group [144] demonstrated that as a result of TP absorption in the 700-850 nm wavelength range, fluorescence emission of hemoglobin and heme solutions can be observed, and the fluorescence relaxation time is less than 50 ps. In study [145] it was demonstrated that the presence of this fluorescence is associated with an irreversible accumulation of a fluorescent photoproduct formed by the spontaneous conversion of a heme molecule in an excited state.

The possibility of non-invasive access to skin cells, primarily in the epidermis, allows to analyze the intercellular biochemical processes, for example, by MI. In particular, using the MPM-FLIM method, it was demonstrated that in keratinocytes during their differentiation the main type of metabolism changes from glycolysis to OP [146]. On the basis of MPM-FLIM, methods for detecting skin cancer, in particular, basal carcinoma [147] and melanoma [63, 104], were also developed.

The analysis of literature conducted in this review allows us to draw the following conclusions. The directions of development for molecular imaging methods are dictated by the needs of fundamental biomedical research and the desire to use it in clinical diagnostics. Despite the fact that MPM is considered, first of all, as a tool that allows 3D scanning of objects using exogenous probes that provide the best specificity and depth of imaging, its application with endogenous contrasts also has its niche. In the field of *in vitro* experiments, the most widely used method is fluorescent metabolic imaging, which is associated both with the value of information that can be obtained by it and with the fact that the biochemical processes underlying it are well-studied. However, even in this direction, unsolved problems remain [61]. For wider use of MPM in experiments *in vitro*, it is necessary to be able to isolate the signal specifically from certain molecules, i.e., isolate the contribution of given fluorophores (for example, lipofuscin, riboflavin, oxidized proteins) from the total signal, which can significantly increase the informative value of the method [101]. In this regard, the

research of photophysical and photochemical processes in endogenous fluorophores, in particular, in heterogeneous fluorophore systems – melanin, lipofuscin, oxidized proteins, and lipids – is relevant. The second task is the development of physical methods for selective imaging of molecules of a given type for expanding MPM capabilities, for example, CARS.

In the field of clinical applications, the main drawback of MPM is the insufficient imaging depth, which limits its use *in vivo* for humans to mainly skin. Despite the presence of a number of studies on the implementation of morphological studies using MPM with endogenous contrasts *ex vivo*, it seems questionable whether this approach will be able to surpass the usual histology, which can also be automated, in sensitivity and specificity. Significant progress could probably be achieved by implementing MPM as an endoscopic technique, allowing its use at least for the same tasks as fluorescence spectroscopy, Raman spectroscopy, and diffuse reflectance spectroscopy. In perspective, new results can be expected from using the groundwork obtained in experiments *in vitro* by MPM with endogenous contrasts on humans *in vivo*.

Funding

This study was supported by the Russian Science Foundation (grant no. 18-15-00422).

REFERENCES

1. Konig, K., and Riemann, I. (2003) High-resolution multiphoton tomography of human skin with subcellular spatial resolution and picosecond time resolution, *J. Biomed. Opt.*, **8**, 432-439.
2. Marcu, L., French, P. M. W., and Elson, D. S. (2014) *Fluorescence Lifetime Spectroscopy and Imaging: Principles and Applications in Biomedical Diagnostics*, CRC Press/Taylor & Francis Group, Boca Raton.
3. Becker, W. (2012) Fluorescence lifetime imaging – techniques and applications, *J. Microsc.*, **247**, 119-136.
4. Helmchen, F., and Denk, W. (2005) Deep tissue two-photon microscopy, *Nat. Methods*, **2**, 932.
5. So, P. T. C., Dong, C. Y., Masters, B. R., and Berland, K. M. (2000) Two-photon excitation fluorescence microscopy, *Annu. Rev. Biomed. Eng.*, **2**, 399-429.
6. Phan, T. G., and Bullen, A. (2010) Practical intravital two-photon microscopy for immunological research: faster, brighter, deeper, *Immunol. Cell. Biol.*, **88**, 438-44.
7. Xu, C., and Zipfel, W. R. (2015) Multiphoton excitation of fluorescent probes, *Cold Spring Harb. Protoc.*, **2015**, doi: 10.1101/pdb.top086116.
8. Zubova, N. N., and Savitzky, A. P. (2005) Molecular cellular sensors, based on colorful fluorescent proteins I: pH sensors, ions of Cl^{-}, Ca^{2+}, Zn^{2+}, Cu^{2+}, *Uspekhi Biol. Khim.*, **45**, 391-454.
9. Mayevsky, A., and Rogatsky, G. G. (2007) Mitochondrial function *in vivo* evaluated by NADH fluorescence: from animal models to human studies, *Am. J. Physiol. Cell Physiol.*, **292**, C615-640.
10. Kolenc, O. I., and Quinn, K. P. (2018) Evaluating cell metabolism through autofluorescence imaging of NAD(P)H and FAD, *Antioxid. Redox Signal*, doi: 10.1089/ars.2017.7451.
11. Obeidy, P., Tong, P. L., and Weninger, W. (2018) Research techniques made simple: two-photon intravital imaging of the skin, *J. Invest. Dermatol.*, **138**, 720-725.
12. Croce, A. C., and Bottiroli, G. (2017) Autofluorescence spectroscopy for monitoring metabolism in animal cells and tissues, *Methods Mol. Biol.*, **1560**, 15-43.
13. Lakowicz, J. R. (2006) *Principles of Fluorescence Spectroscopy*, 3rd Edn., Springer, New York.
14. Berezin, M. Y., and Achilefu, S. (2010) Fluorescence lifetime measurements and biological imaging, *Chem. Rev.*, **110**, 2641-84.
15. Pavone, F. S., and Campagnola, P. J. (2014) *Second Harmonic Generation Imaging*, CRC Press Taylor & Francis, Boca Raton.
16. Akhmanov, S. A., and Nikitin, S. Yu. (2004) *Physical Optics* [in Russian], MSU Publishers, Moscow.
17. Shen, Y.-R. (1984) *The Principles of Nonlinear Optics*, Wiley-Interscience, New York.
18. Sdobnov, A. Y., Darvin, M. E., Genina, E. A., Bashkatov, A. N., Lademann, J., and Tuchin, V. V. (2018) Recent progress in tissue optical clearing for spectroscopic application, *Spectrochim. Acta A Mol. Biomol. Spectrosc.*, **197**, 216-229.
19. Oheim, M., Beaurepaire, E., Chaigneau, E., Mertz, J., and Charpak, S. (2001) Two-photon microscopy in brain tissue: parameters influencing the imaging depth, *J. Neurosci. Methods*, **111**, 29-37.
20. Oheim, M., Michael, D. J., Geisbauer, M., Madsen, D., and Chow, R. H. (2006) Principles of two-photon excitation fluorescence microscopy and other nonlinear imaging approaches, *Adv. Drug Deliv. Rev.*, **58**, 788-808.
21. Boyd, R. W. (2003) *Nonlinear Optics*, Elsevier, Amsterdam.
22. Steinfeld, J. I. (2012) *Molecules and Radiation: an Introduction to Modern Molecular Spectroscopy*, Courier Corporation, North Chelmsford.
23. Campagnola, P. J., and Loew, L. M. (2003) Second-harmonic imaging microscopy for visualizing biomolecular arrays in cells, tissues and organisms, *Nat. Biotechnol.*, **21**, 1356-1360.
24. Masters, B. R., and So, P. (2008) *Handbook of Biomedical Nonlinear Optical Microscopy*, Oxford University Press, Oxford.
25. Muller, M., and Zumbusch, A. (2007) Coherent anti-Stokes Raman scattering microscopy, *ChemPhysChem*, **8**, 2156-2170.
26. Cheng, J.-X., and Xie, X. S. (2004) Coherent anti-Stokes Raman scattering microscopy: instrumentation, theory, and applications, *J. Phys. Chem. B*, **108**, 827-840.
27. Xie, X. S., Cheng, J.-X., and Potma, E. (2006) Coherent anti-Stokes Raman scattering microscopy, in *Handbook of Biological Confocal Microscopy* (Pawley, J., ed.), Springer, Boston, pp. 595-606.
28. Bashkatov, A. N., Genina, E. A., and Tuchin, V. V. (2011) Optical properties of skin, subcutaneous, and muscle tissues: a review, *J. Innov. Opt. Health Sci.*, **4**, 9-38.

29. Xu, C., Zipfel, W., Shear, J. B., Williams, R. M., and Webb, W. W. (1996) Multiphoton fluorescence excitation: new spectral windows for biological nonlinear microscopy, *Proc. Natl. Acad. Sci. USA*, **93**, 10763-10768.
30. Hopt, A., and Neher, E. (2001) Highly nonlinear photodamage in two-photon fluorescence microscopy, *Biophys. J.*, **80**, 2029-2036.
31. Zipfel, W. R., Williams, R. M., and Webb, W. W. (2003) Nonlinear magic: multiphoton microscopy in the biosciences, *Nat. Biotechnol.*, **21**, 1369-1377.
32. Balu, M., Baldacchini, T., Carter, J. L., Krasieva, T. B., Zadoyan, R., and Tromberg, B. J. (2009) Effect of excitation wavelength on penetration depth in nonlinear optical microscopy of turbid media, *J. Biomed. Opt.*, **14**, 010508.
33. Kobat, D., Horton, N. G., and Xu, C. (2011) *In vivo* two-photon microscopy to 1.6-mm depth in mouse cortex, *J. Biomed. Opt.*, **16**, 106014.
34. Theer, P., and Denk, W. (2006) On the fundamental imaging-depth limit in two-photon microscopy, *JOSA A*, **23**, 3139-3149.
35. Majewska, A., Yiu, G., and Yuste, R. (2000) A custom-made two-photon microscope and deconvolution system, *Pflugers Arch.*, **441**, 398-408.
36. Nguyen, Q. T., Callamaras, N., Hsieh, C., and Parker, I. (2001) Construction of a two-photon microscope for video-rate Ca^{2+} imaging, *Cell Calcium*, **30**, 383-393.
37. Periasamy, A., and Clegg, R. M. (2009) *FLIM Microscopy in Biology and Medicine*, Chapman and Hall/CRC, New York.
38. Kollner, M., and Wolfrum, J. (1992) How many photons are necessary for fluorescence-lifetime measurements? *Chem. Phys. Lett.*, **200**, 199-204.
39. Digman, M. A., Caiolfa, V. R., Zamai, M., and Gratton, E. (2008) The phasor approach to fluorescence lifetime imaging analysis, *Biophys. J.*, **94**, L14-L16.
40. Le Marois, A., Labouesse, S., Suhling, K., and Heintzmann, R. (2017) Noise-corrected principal component analysis of fluorescence lifetime imaging data, *J. Biophotonics*, **10**, 1124-1133.
41. Leray, A., Padilla-Parra, S., Roul, J., Heliot, L., and Tramier, M. (2013) Spatio-temporal quantification of FRET in living cells by fast time-domain FLIM: a comparative study of non-fitting methods, *PloS One*, **8**, e69335.
42. Stringari, C., Cinquin, A., Cinquin, O., Digman, M. A., Donovan, P. J., and Gratton, E. (2011) Phasor approach to fluorescence lifetime microscopy distinguishes different metabolic states of germ cells in a live tissue, *Proc. Natl. Acad. Sci. USA*, **108**, 13582-13587.
43. Ranjit, S., Dvornikov, A., Stakic, M., Hong, S. H., Levi, M., Evans, R. M., and Gratton, E. (2015) Imaging fibrosis and separating collagens using second harmonic generation and phasor approach to fluorescence lifetime imaging, *Sci. Rep.*, **5**, 13378.
44. Zhdanova, N. G., Shirshin, E. A., Maksimov, E. G., Panchishin, I. M., Saletsky, A. M., and Fadeev, V. V. (2015) Tyrosine fluorescence probing of the surfactant-induced conformational changes of albumin, *Photochem. Photobiol. Sci.*, **14**, 897-908.
45. Li, C., Pistillides, C., Runnels, J. M., Cote, D., and Li, C. (2010) Multiphoton microscopy of live tissues with ultraviolet autofluorescence, *IEEE J. Sel. Top. Quantum Electron.*, **16**, 516-523.
46. Li, C., Pastila, R. K., Pitsillides, C., Runnels, J. M., Puoris'haag, M., Cote, D., and Lin, C. P. (2010) Imaging leukocyte trafficking *in vivo* with two-photon-excited endogenous tryptophan fluorescence, *Opt. Express*, **18**, 988-999.
47. Alam, S. R., Wallrabe, H., Svindrych, Z., Chaudhary, A. K., Christopher, K. G., Chandra, D., and Periasamy, A. (2017) Investigation of mitochondrial metabolic response to doxorubicin in prostate cancer cells: an NADH, FAD and tryptophan FLIM assay, *Sci. Rep.*, **7**, 10451.
48. Jyothikumar, V., Sun, Y., and Periasamy, A. (2013) Investigation of tryptophan-NADH interactions in live human cells using three-photon fluorescence lifetime imaging and Forster resonance energy transfer microscopy, *J. Biomed. Opt.*, **18**, 060501.
49. Maiti, S., Shear, J. B., Williams, R. M., Zipfel, W. R., and Webb, W. W. (1997) Measuring serotonin distribution in live cells with three-photon excitation, *Science*, **275**, 530-532.
50. Vivian, J. T., and Callis, P. R. (2001) Mechanisms of tryptophan fluorescence shifts in proteins, *Biophys. J.*, **80**, 2093-2109.
51. Shirshin, E. A., Gurfinkel, Y. I., Priezzhev, A. V., Fadeev, V. V., Lademann, J., and Darvin, M. E. (2017) Two-photon autofluorescence lifetime imaging of human skin papillary dermis *in vivo*: assessment of blood capillaries and structural proteins localization, *Sci. Rep.*, **7**, 1171.
52. Borisova, E., Angelova, L., and Pavlova, E. (2014) Endogenous and exogenous fluorescence skin cancer diagnostics for clinical applications, *IEEE J. Sel. Top. Quantum Electron.*, **20**, 7100412.
53. Palero, J. A., de Bruijn, H. S., van der Ploeg van den Heuvel, A., Sterenborg, H. J., and Gerritsen, H. C. (2007) Spectrally resolved multiphoton imaging of *in vivo* and excised mouse skin tissues, *Biophys. J.*, **93**, 992-1007.
54. Voloshina, O. V., Shirshin, E. A., Lademann, J., Fadeev, V. V., and Darvin, M. E. (2017) Fluorescence detection of protein content in house dust: the possible role of keratin, *Indoor Air*, **27**, 377-385.
55. Pena, A., Strupler, M., Boulesteix, T., and Schanne-Klein, M. (2005) Spectroscopic analysis of keratin endogenous signal for skin multiphoton microscopy, *Opt. Express*, **13**, 6268-6274.
56. Mulder, D. J., Water, T. V., Lutgers, H. L., Graaff, R., Gans, R. O., Zijlstra, F., and Smit, A. J. (2006) Skin autofluorescence, a novel marker for glycemic and oxidative stress-derived advanced glycation endproducts: an overview of current clinical studies, evidence, and limitations, *Diabetes Technol. Ther.*, **8**, 523-535.
57. Ghazaryan, A. A., Hu, P. S., Chen, S. J., Tan, H. Y., and Dong, C. Y. (2012) Spatial and temporal analysis of skin glycation by the use of multiphoton microscopy and spectroscopy, *J. Dermatol. Sci.*, **65**, 189-195.
58. Blacker, T. S., Mann, Z. F., Gale, J. E., Ziegler, M., Bain, A. J., Szabadkai, G., and Duchen, M. R. (2014) Separating NADH and NADPH fluorescence in live cells and tissues using FLIM, *Nat. Commun.*, **5**, 3936.
59. Huang, S., Heikal, A. A., and Webb, W. W. (2002) Two-photon fluorescence spectroscopy and microscopy of NAD(P)H and flavoprotein, *Biophys. J.*, **82**, 2811-2825.
60. Yu, Q., and Heikal, A. A. (2009) Two-photon autofluorescence dynamics imaging reveals sensitivity of intracellular NADH concentration and conformation to cell physiology

at the single-cell level, *J. Photochem. Photobiol. B*, **95**, 46-57.
61. Blacker, T. S., and Duchen, M. R. (2016) Investigating mitochondrial redox state using NADH and NADPH autofluorescence, *Free Radic. Biol. Med.*, **100**, 53-65.
62. Galban, J., Sanz-Vicente, I., Navarro, J., and de Marcos, S. (2016) The intrinsic fluorescence of FAD and its application in analytical chemistry: a review, *Methods Appl. Fluoresc.*, **4**, 042005.
63. Dimitrow, E., Riemann, I., Ehlers, A., Koehler, M. J., Norgauer, J., Elsner, P., Konig, K., and Kaatz, M. (2009) Spectral fluorescence lifetime detection and selective melanin imaging by multiphoton laser tomography for melanoma diagnosis, *Exp. Dermatol.*, **18**, 509-515.
64. Teuchner, K., Freyer, W., Leupold, D., Volkmer, A., Birch, D. J., Altmeyer, P., Stucker, M., and Hoffmann, K. (1999) Femtosecond two-photon excited fluorescence of melanin, *Photochem. Photobiol.*, **70**, 146-151.
65. Rice, W. L., Kaplan, D. L., and Georgakoudi, I. (2010) Two-photon microscopy for non-invasive, quantitative monitoring of stem cell differentiation, *PLoS One*, **5**, e10075.
66. Chen, C., Liang, Z., Zhou, B., Li, X., Lui, C., Ip, N. Y., and Qu, J. (2018) *In vivo* near-infrared two-photon imaging of amyloid plaques in deep brain of Alzheimer's disease mouse model, *ACS Chem. Neurosci.*, doi: 10.1021/acschemneuro.8b00306.
67. Sinichkin, Y. P., Utz, S. R., Mavliutov, A. H., and Pilipenko, H. A. (1998) *In vivo* fluorescence spectroscopy of the human skin: experiments and models, *J. Biomed. Opt.*, **3**, 201-211.
68. Robins, S. P. (1982) Analysis of the crosslinking components in collagen and elastin, *Methods Biochem. Anal.*, **28**, 329-379.
69. Deyl, Z., Macek, K., Adam, M., and Vancikova, O. (1980) Studies on the chemical nature of elastin fluorescence, *Biochim. Biophys. Acta*, **625**, 248-254.
70. Stamatas, G. N., Estanislao, R. B., Suero, M., Rivera, Z. S., Li, J., Khaiat, A., and Kollias, N. (2006) Facial skin fluorescence as a marker of the skin's response to chronic environmental insults and its dependence on age, *Br. J. Dermatol.*, **154**, 125-132.
71. Malencik, D. A., and Anderson, S. R. (2003) Dityrosine as a product of oxidative stress and fluorescent probe, *Amino Acids*, **25**, 233-247.
72. Sterenborg, N. J., Thomsen, S., Jacques, S. L., Duvic, M., Motamedi, M., and Wagner, R. F., Jr. (1995) *In vivo* fluorescence spectroscopy and imaging of human skin tumors, *Dermatol. Surg.*, **21**, 821-822.
73. Marcu, L., Cohen, D., Maarek, J.-M., and Grundfest, W. (2000) Characterization of type I, II, III, IV, and V collagens by time-resolved laser-induced fluorescence spectroscopy, *Proc. SPIE*, **3917**, 93-101.
74. Choe, C., Schleusener, J., Lademann, J., and Darvin, M. E. (2017) Keratin–water–NMF interaction as a three layer model in the human stratum corneum using *in vivo* confocal Raman microscopy, *Sci. Rep.*, **7**, 15900.
75. Gkogkolou, P., and Bohm, M. (2012) Advanced glycation end products: key players in skin aging? *Dermatoendocrinology*, **4**, 259-270.
76. Dyer, D. G., Dunn, J. A., Thorpe, S. R., Bailie, K. E., Lyons, T. J., McCance, D. R., and Baynes, J. W. (1993) Accumulation of Maillard reaction products in skin collagen in diabetes and aging, *J. Clin. Invest.*, **91**, 2463-2469.
77. Dyer, D. G., Blackledge, J. A., Thorpe, S. R., and Baynes, J. W. (1991) Formation of pentosidine during nonenzymatic browning of proteins by glucose. Identification of glucose and other carbohydrates as possible precursors of pentosidine *in vivo*, *J. Biol. Chem.*, **266**, 11654-11660.
78. Monnier, V. M., Kohn, R. R., and Cerami, A. (1984) Accelerated age-related browning of human collagen in diabetes mellitus, *Proc. Natl. Acad. Sci. USA*, **81**, 583-587.
79. Kim, B. M., Eichler, J., Reiser, K. M., Rubenchik, A. M., and Da Silva, L. B. (2000) Collagen structure and nonlinear susceptibility: effects of heat, glycation, and enzymatic cleavage on second harmonic signal intensity, *Lasers Surg. Med.*, **27**, 329-335.
80. Tseng, J. Y., Ghazaryan, A. A., Lo, W., Chen, Y. F., Hovhannisyan, V., Chen, S. J., Tan, H. Y., and Dong, C. Y. (2010) Multiphoton spectral microscopy for imaging and quantification of tissue glycation, *Biomed. Opt. Express*, **2**, 218-230.
81. Dyer, J. M., Bringans, S. D., and Bryson, W. G. (2006) Characterisation of photo-oxidation products within photoyellowed wool proteins: tryptophan and tyrosine derived chromophores, *Photochem. Photobiol. Sci.*, **5**, 698-706.
82. Pattison, D. I., Rahmanto, A. S., and Davies, M. J. (2012) Photo-oxidation of proteins, *Photochem. Photobiol. Sci.*, **11**, 38-53.
83. Balasubramanian, D., and Kanwar, R. (2002) Molecular pathology of dityrosine cross-links in proteins: structural and functional analysis of four proteins, *Mol. Cell. Biochem.*, **234-235**, 27-38.
84. Soskic, V., Groebe, K., and Schrattenholz, A. (2008) Nonenzymatic posttranslational protein modifications in ageing, *Exp. Gerontol.*, **43**, 247-257.
85. Tikhonova, T. N., Rovnyagina, N. R., Zherebker, A. Y., Sluchanko, N. N., Rubekina, A. A., Orekhov, A. S., Nikolaev, E. N., Fadeev, V. V., Uversky, V. N., and Shirshin, E. A. (2018) Dissection of the deep-blue autofluorescence changes accompanying amyloid fibrillation, *Arch. Biochem. Biophys.*, **651**, 13-20.
86. Pinotsi, D., Buell, A. K., Dobson, C. M., Kaminski Schierle, G. S., and Kaminski, C. F. (2013) A label-free, quantitative assay of amyloid fibril growth based on intrinsic fluorescence, *Chembiochem*, **14**, 846-850.
87. Shukla, A., Mukherjee, S., Sharma, S., Agrawal, V., Radha Kishan, K. V., and Guptasarma, P. (2004) A novel UV laser-induced visible blue radiation from protein crystals and aggregates: scattering artifacts or fluorescence transitions of peptide electrons delocalized through hydrogen bonding? *Arch. Biochem. Biophys.*, **428**, 144-153.
88. Shaham-Niv, S., Arnon, Z. A., Sade, D., Lichtenstein, A., Shirshin, E. A., Kolusheva, S., and Gazit, E. (2018) Intrinsic fluorescence of metabolite amyloids allows label-free monitoring of their formation and dynamics in live cells, *Angew. Chem. Int. Ed. Engl.*, **57**, 12444-12447.
89. Pinotsi, D., Grisanti, L., Mahou, P., Gebauer, R., Kaminski, C. F., Hassanali, A., and Kaminski Schierle, G. S. (2016) Proton transfer and structure-specific fluorescence in hydrogen bond-rich protein structures, *J. Am. Chem. Soc.*, **138**, 3046-3057.
90. Niyangoda, C., Miti, T., Breydo, L., Uversky, V., and Muschol, M. (2017) Carbonyl-based blue autofluorescence of proteins and amino acids, *PLoS One*, **12**, e0176983.

91. Permyakov, E. A., Permyakov, S. E., Deikus, G. Y., Morozova-Roche, L. A., Grishchenko, V. M., Kalinichenko, L. P., and Uversky, V. N. (2003) Ultraviolet illumination-induced reduction of alpha-lactalbumin disulfide bridges, *Proteins*, **51**, 498-503.
92. Ying, W. (2008) NAD^+/NADH and $NADP^+$/NADPH in cellular functions and cell death: regulation and biological consequences, *Antioxid. Redox. Signal.*, **10**, 179-206.
93. Blacker, T. S., Berecz, T., Duchen, M. R., and Szabadkai, G. (2017) Assessment of cellular redox state using NAD(P)H fluorescence intensity and lifetime, *Bio Protoc.*, **7**, e2105.
94. Vishwasrao, H. D., Heikal, A. A., Kasischke, K. A., and Webb, W. W. (2005) Conformational dependence of intracellular NADH on metabolic state revealed by associated fluorescence anisotropy, *J. Biol. Chem.*, **280**, 25119-25126.
95. Visser, A. J. W. G., and van Hoek, A. (1981) The fluorescence decay of reduced nicotinamides in aqueous solution after excitation with a UV-mode locked Ar ion laser, *Photochem. Photobiol.*, **33**, 35-40.
96. Blacker, T., Marsh, R. J., Duchen, M. R., and Bain, A. J. (2013) Activated barrier crossing dynamics in the non-radiative decay of NADH and NADPH, *Chem. Phys.*, **422**, 184-194.
97. Skala, M. C., Riching, K. M., Gendron-Fitzpatrick, A., Eickhoff, J., Eliceiri, K. W., White, J. G., and Ramanujam, N. (2007) *In vivo* multiphoton microscopy of NADH and FAD redox states, fluorescence lifetimes, and cellular morphology in precancerous epithelia, *Proc. Natl. Acad. Sci. USA*, **104**, 19494-19499.
98. Kunz, W. S., and Kunz, W. (1985) Contribution of different enzymes to flavoprotein fluorescence of isolated rat liver mitochondria, *Biochim. Biophys. Acta*, **841**, 237-246.
99. Mataga, N., Chosrowjan, H., and Shibata, Y. (2000) Dynamics and mechanisms of ultrafast fluorescence quenching reactions of flavin chromophores in protein nanospace, *J. Phys. Chem. B*, **104**, 10667-10677.
100. Lukina, M. M., Shirmanova, M. V., Sergeeva, T. F., and Zagaynova, E. V. (2016) Metabolic imaging in the study of oncological processes (review), *Sovrem. Tekhnol. Med.*, **8**, 113-126.
101. Miranda-Lorenzo, I., Dorado, J., Lonardo, E., Alcala, S., Serrano, A. G., Clausell-Tormos, J., Cioffi, M., Megias, D., Zagorac, S., Balic, A., Hidalgo, M., Erkan, M., Kleeff, J., Scarpa, A., Sainz, B., Jr., and Heeschen, C. (2014) Intracellular autofluorescence: a biomarker for epithelial cancer stem cells, *Nat. Methods*, **11**, 1161-1169.
102. Solano, F. (2014) Melanins: skin pigments and much more – types, structural models, biological functions, and formation, *New J. Sci.*, **2014**, 498276.
103. Huang, Z., Zeng, H., Hamzavi, I., Alajlan, A., Tan, E., McLean, D. I., and Lui, H. (2006) Cutaneous melanin exhibiting fluorescence emission under near-infrared light excitation, *J. Biomed. Opt.*, **11**, 34010.
104. Arginelli, F., Manfredini, M., Bassoli, S., Dunsby, C., French, P., Konig, K., Magnoni, C., Ponti, G., Talbot, C., and Seidenari, S. (2013) High resolution diagnosis of common nevi by multiphoton laser tomography and fluorescence lifetime imaging, *Skin Res. Technol.*, **19**, 194-204.
105. Wolman, M. (1980) Lipid pigments (chromolipids): their origin, nature, and significance, *Pathobiol. Annu.*, **10**, 253-267.
106. Terman, A., Kurz, T., Navratil, M., Arriaga, E. A., and Brunk, U. T. (2010) Mitochondrial turnover and aging of long-lived postmitotic cells: the mitochondrial-lysosomal axis theory of aging, *Antioxid. Redox Signal.*, **12**, 503-535.
107. Di Guardo, G. (2015) Lipofuscin, lipofuscin-like pigments and autofluorescence, *Eur. J. Histochem.*, **59**, 2485.
108. Yin, D. Z., and Brunk, U. T. (1991) Microfluorometric and fluorometric lipofuscin spectral discrepancies: a concentration-dependent metachromatic effect? *Mech. Ageing Dev.*, **59**, 95-109.
109. Schnell, S. A., Staines, W. A., and Wessendorf, M. W. (1999) Reduction of lipofuscin-like autofluorescence in fluorescently labeled tissue, *J Histochem. Cytochem.*, **47**, 719-730.
110. Cicchi, R., Vogler, N., Kapsokalyvas, D., Dietzek, B., Popp, J., and Pavone, F. S. (2013) From molecular structure to tissue architecture: collagen organization probed by SHG microscopy, *J. Biophotonics*, **6**, 129-142.
111. Darvin, M. E., Konig, K., Kellner-Hoefer, M., Breunig, H. G., Werncke, W., Meinke, M. C., Patzelt, A., Sterry, W., and Lademann, J. (2012) Safety assessment by multiphoton fluorescence/second harmonic generation/hyper-Rayleigh scattering tomography of ZnO nanoparticles used in cosmetic products, *Skin Pharmacol. Physiol.*, **25**, 219-226.
112. Chang, T., Zimmerley, M. S., Quinn, K. P., Lamarre-Jouenne, I., Kaplan, D. L., Beaurepaire, E., and Georgakoudi, I. (2013) Non-invasive monitoring of cell metabolism and lipid production in 3D engineered human adipose tissues using label-free multiphoton microscopy, *Biomaterials*, **34**, 8607-8616.
113. Weigelin, B., Bakker, G. J., and Friedl, P. (2016) Third harmonic generation microscopy of cells and tissue organization, *J. Cell Sci.*, **129**, 245-255.
114. Debarre, D., Supatto, W., Pena, A. M., Fabre, A., Tordjmann, T., Combettes, L., Schanne-Klein, M. C., and Beaurepaire, E. (2006) Imaging lipid bodies in cells and tissues using third-harmonic generation microscopy, *Nat. Methods*, **3**, 47-53.
115. You, S., Tu, H., Chaney, E. J., Sun, Y., Zhao, Y., Bower, A. J., Liu, Y. Z., Marjanovic, M., Sinha, S., Pu, Y., and Boppart, S. A. (2018) Intravital imaging by simultaneous label-free autofluorescence-multiharmonic microscopy, *Nat. Commun.*, **9**, 2125.
116. Lakowicz, J. R., Szmacinski, H., Nowaczyk, K., and Johnson, M. L. (1992) Fluorescence lifetime imaging of free and protein-bound NADH, *Proc. Natl. Acad. Sci. USA*, **89**, 1271-1275.
117. Walsh, A. J., Shah, A. T., Sharick, J. T., and Skala, M. C. (2015) Fluorescence lifetime measurements of NAD(P)H in live cells and tissue, in *Advanced Time-Correlated Single Photon Counting Applications* (Becker, W., ed.) Springer International Publishing, Cham, pp. 435-456.
118. Lopez-Lazaro, M. (2008) The warburg effect: why and how do cancer cells activate glycolysis in the presence of oxygen? *Anticancer Agents Med. Chem.*, **8**, 305-312.
119. Berridge, M. V., Herst, P. M., and Tan, A. S. (2010) Metabolic flexibility and cell hierarchy in metastatic cancer, *Mitochondrion*, **10**, 584-588.
120. Datta, R., Alfonso-Garcia, A., Cinco, R., and Gratton, E. (2015) Fluorescence lifetime imaging of endogenous biomarker of oxidative stress, *Sci. Rep.*, **5**, 9848.

121. Stringari, C., Edwards, R. A., Pate, K. T., Waterman, M. L., Donovan, P. J., and Gratton, E. (2012) Metabolic trajectory of cellular differentiation in small intestine by phasor fluorescence lifetime microscopy of NADH, *Sci. Rep.*, **2**, 568.
122. Stringari, C., Sierra, R., Donovan, P. J., and Gratton, E. (2012) Label-free separation of human embryonic stem cells and their differentiating progenies by phasor fluorescence lifetime microscopy, *J. Biomed. Opt.*, **17**, 046012.
123. Stringari, C., Nourse, J. L., Flanagan, L. A., and Gratton, E. (2012) Phasor fluorescence lifetime microscopy of free and protein-bound NADH reveals neural stem cell differentiation potential, *PLoS One*, **7**, e48014.
124. Wright, B. K., Andrews, L. M., Markham, J., Jones, M. R., Stringari, C., Digman, M. A., and Gratton, E. (2012) NADH distribution in live progenitor stem cells by phasor-fluorescence lifetime image microscopy, *Biophys. J.*, **103**, L7-9.
125. Kim, J. H., Cho, E. J., Kim, S. T., and Youn, H. D. (2005) CtBP represses p300-mediated transcriptional activation by direct association with its bromodomain, *Nat. Struct. Mol. Biol.*, **12**, 423-428.
126. Wright, B. K., Andrews, L. M., Jones, M. R., Stringari, C., Digman, M. A., and Gratton, E. (2012) Phasor-FLIM analysis of NADH distribution and localization in the nucleus of live progenitor myoblast cells, *Microsc. Res. Tech.*, **75**, 1717-1722.
127. Stringari, C., Wang, H., Geyfman, M., Crosignani, V., Kumar, V., Takahashi, J. S., Andersen, B., and Gratton, E. (2015) *In vivo* single-cell detection of metabolic oscillations in stem cells, *Cell Rep.*, **10**, 1-7.
128. Datta, R., Heylman, C., George, S. C., and Gratton, E. (2016) Label-free imaging of metabolism and oxidative stress in human induced pluripotent stem cell-derived cardiomyocytes, *Biomed. Opt. Express*, **7**, 1690-1701.
129. Santin, G., Paulis, M., Vezzoni, P., Pacchiana, G., Bottiroli, G., and Croce, A. C. (2013) Autofluorescence properties of murine embryonic stem cells during spontaneous differentiation phases, *Lasers Surg. Med.*, **45**, 597-607.
130. Osellame, L. D., Blacker, T. S., and Duchen, M. R. (2012) Cellular and molecular mechanisms of mitochondrial function, *Best Pract. Res. Clin. Endocrinol. Metab.*, **26**, 711-723.
131. Scott, D. A., Tabarean, I., Tang, Y., Cartier, A., Masliah, E., and Roy, S. (2010) A pathologic cascade leading to synaptic dysfunction in alpha-synuclein-induced neurodegeneration, *J. Neurosci.*, **30**, 8083-8095.
132. Plotegher, N., Stringari, C., Jahid, S., Veronesi, M., Girotto, S., Gratton, E., and Bubacco, L. (2015) NADH fluorescence lifetime is an endogenous reporter of alpha-synuclein aggregation in live cells, *FASEB J.*, **29**, 2484-2494.
133. Chakraborty, S., Nian, F. S., Tsai, J. W., Karmenyan, A., and Chiou, A. (2016) Quantification of the metabolic state in cell-model of Parkinson's disease by fluorescence lifetime imaging microscopy, *Sci. Rep.*, **6**, 19145.
134. Przedborski, S., Tieu, K., Perier, C., and Vila, M. (2004) MPTP as a mitochondrial neurotoxic model of Parkinson's disease, *J. Bioenerg. Biomembr.*, **36**, 375-379.
135. Sameni, S., Syed, A., Marsh, J. L., and Digman, M. A. (2016) The phasor-FLIM fingerprints reveal shifts from OXPHOS to enhanced glycolysis in Huntington disease, *Sci. Rep.*, **6**, 34755.
136. Marsh, J. L., Pallos, J., and Thompson, L. M. (2003) Fly models of Huntington's disease, *Hum. Mol. Genet.*, **12**, Special No. 2, R187-193.
137. Shirshin, E. A., Gurfinkel, Y. I., Matskeplishvili, S. T., Sasonko, M. L., Omelyanenko, N. P., Yakimov, B. P., Lademann, J., and Darvin, M. E. (2018) *In vivo* optical imaging of the viable epidermis around the nailfold capillaries for the assessment of heart failure severity in humans, *J. Biophotonics*, **11**, e201800066.
138. Huck, V., Gorzelanny, C., Thomas, K., Getova, V., Niemeyer, V., Zens, K., Unnerstall, T. R., Feger, J. S., Fallah, M. A., Metze, D., Stander, S., Luger, T. A., Koenig, K., Mess, C., and Schneider, S. W. (2016) From morphology to biochemical state – intravital multiphoton fluorescence lifetime imaging of inflamed human skin, *Sci. Rep.*, **6**, 22789.
139. Pouli, D., Balu, M., Alonzo, C. A., Liu, Z., Quinn, K. P., Rius-Diaz, F., Harris, R. M., Kelly, K. M., Tromberg, B. J., and Georgakoudi, I. (2016) Imaging mitochondrial dynamics in human skin reveals depth-dependent hypoxia and malignant potential for diagnosis, *Sci. Transl. Med.*, **8**, 367ra169.
140. Klemp, M., Meinke, M. C., Weinigel, M., Rowert-Huber, H. J., Konig, K., Ulrich, M., Lademann, J., and Darvin, M. E. (2016) Comparison of morphologic criteria for actinic keratosis and squamous cell carcinoma using *in vivo* multiphoton tomography, *Exp. Dermatol.*, **25**, 218-222.
141. Yokouchi, M., Atsugi, T., Logtestijn, M. V., Tanaka, R. J., Kajimura, M., Suematsu, M., Furuse, M., Amagai, M., and Kubo, A. (2016) Epidermal cell turnover across tight junctions based on Kelvin's tetrakaidecahedron cell shape, *Elife*, **5**, e19593.
142. Newton, V. L., Bradley, R. S., Seroul, P., Cherel, M., Griffiths, C. E., Rawlings, A. V., Voegeli, R., Watson, R. E., and Sherratt, M. J. (2017) Novel approaches to characterize age-related remodelling of the dermal-epidermal junction in 2D, 3D and *in vivo*, *Skin Res. Technol.*, **23**, 131-148.
143. Springer, S., Zieger, M., Koenig, K., Kaatz, M., Lademann, J., and Darvin, M. E. (2016) Optimization of the measurement procedure during multiphoton tomography of human skin *in vivo*, *Skin Res. Technol.*, **22**, 356-362.
144. Sun, Q., Zheng, W., Wang, J., Luo, Y., and Qu, J. Y. (2015) Mechanism of two-photon excited hemoglobin fluorescence emission, *J. Biomed. Opt.*, **20**, 105014.
145. Shirshin, E. A., Yakimov, B. P., Rodionov, S. A., Omelyanenko, N. P., Priezzhev, A. V., Fadeev, V. V., Lademann, J., and Darvin, M. E. (2018) Formation of hemoglobin photoproduct is responsible for two-photon and single photon-excited fluorescence of red blood cells, *Laser. Phys. Lett.*, **15**, 075604.
146. Stringari, C., Abdeladim, L., Malkinson, G., Mahou, P., Solinas, X., Lamarre, I., Brizion, S., Galey, J. B., Supatto, W., Legouis, R., Pena, A. M., and Beaurepaire, E. (2017) Multicolor two-photon imaging of endogenous fluorophores in living tissues by wavelength mixing, *Sci. Rep.*, **7**, 3792.
147. Patalay, R., Talbot, C., Alexandrov, Y., Lenz, M. O., Kumar, S., Warren, S., Munro, I., Neil, M. A., Konig, K., French, P. M., Chu, A., Stamp, G. W., and Dunsby, C. (2012) Multiphoton multispectral fluorescence lifetime tomography for the evaluation of basal cell carcinomas, *PLoS One*, **7**, e43460.